DEVELOPMENT OF NYLON-6/GRAPHENE OXIDE (GO) HIGH PERFORMANCE NANOCOMPOSITES

TAY YI HUI

A project report submitted in partial fulfilment of the requirements for the award of the degree of Bachelor of Engineering (Hons) Petrochemical Engineering

Faculty of Engineering and Green Technology
Universiti Tunku Abdul Rahman

September 2015

DECLARATION

I hereby declare that this project report is based on my original work except for citations and quotations which have been duly acknowledged. I also declare that it has not been previously and concurrently submitted for any other degree or award at UTAR or other institutions.

Signature : _____

Name : _____

ID No. : _____

Date : _____

APPROVAL FOR SUBMISSION

I certify that this project report entitled **"DEVELOPMENT OF NYLON-6/GRAPHENE OXIDE (GO) HIGH PERFORMANCE NANOCOMPOSITES"** was prepared by **TAY YI HUI** has met the required standard for submission in partial fulfilment of the requirements for the award of Bachelor of Engineering (Hons) Petrochemical Engineering at Universiti Tunku Abdul Rahman.

Approved by,

Signature : _____

Supervisor : Dr. Yamuna a/p Munusamy

Date : _____

ACKNOWLEDGEMENTS

I would like to express my outmost gratitude to my research supervisor, Dr. Yamuna Munusamy for her guidance throughout the development of the research. I would also like to thank the lecturers and staffs of UTAR especially Dr Mathialagan and Mr Yong Tzyy Jeng who had given me a lot of assistance and advice during the course of the project.

Last but not least, I would also like to express my gratitude to HVW Technologies and Platinum Senawang Sdn Bhd for their research support.

DEVELOPMENT OF NYLON-6/GRAPHENE OXIDE (GO) HIGH PERFORMANCE NANOCOMPOSITES

ABSTRACT

Polymer nanocomposites have been gaining much attention in producing high strength materials due to the low cost and process ability of polymers. In this study, nylon-6/graphene oxide (GO) nanocomposites were developed and characterized. Graphite oxide was synthesized from graphite nanofibre (GNF) using conventional Hummer's Method. It was characterized by Fourier Transform Infrared Spectroscopy (FTIR), X-ray Photoelectron Spectroscopy (XPS), Raman Spectroscopy, X-Ray Diffraction (XRD), Field Emission Scanning Electron Microscopy (FESEM) and Thermal Gravimetric Analysis (TGA). These characterizations proved the successful oxidation of GNF. Graphite oxide was infused into nylon-6 to produce nylon-6/GO nanocomposites at loadings of 0.5, 1.0, 1.5 and 2.0wt% through melt mixing method. The nanocomposites were characterized by FTIR, Differential Scanning Calorimetry (DSC) and TGA. FTIR evidenced the presence of GO and hydrogen bond formation between GO and nylon-6. There was not much difference in melting temperatures of the nanocomposites compared to virgin nylon-6 sample as obtained from DSC data. Melt Flow Index (MFI) was also done to measure the melt flow rate (MFR) of the nanocomposites. The MFR of the nanocomposites reduced slightly by 1.55% to 2.66% with no significant change compared to MFR of pure nylon-6. This indicated the similar processability of the nylon-6 and nylon-6/GO nanocomposites. TGA denoted higher thermal stability of the nanocomposites with shifting of the onset decomposition temperature by roughly 25^{o}C with addition of 2.0wt% GO. Mechanical properties of the nanocomposites were investigated by tensile test. Results showed that the Young's Modulus and tensile strength of nanocomposites at 2.0wt% GO loading were the highest, with enhancement of 30.7% and 23.8% respectively. Meanwhile, the elongation at break dropped for 85.87 % compared to

virgin nylon-6. The cross sectional morphology of the fractured nanocomposites after tensile test was examined by FESEM. Good dispersion of GO, more matrix tearing and deflection of crack growth from the major fracture surface could be observed in the nanocomposites. These two factors contributed to the enhancement in tensile strength and modulus of the nanocomposites. Lastly, water absorbing ability of the nanocomposites was investigated. The increment in weight of nylon-6 decreased from 11.83% to 8.95% as 2.0wt% of GO was used, indicating stronger water resistance.

Keywords: Graphene oxide; Nylon-6; Nanocomposite; Thermal Properties; Mechanical Properties

TABLE OF CONTENTS

LIST OF TABLES

LIST OF FIGURES

LIST OF SYMBOLS / ABBREVIATIONS

PNC	polymer nanocomposite
CNT	carbon nanotube
SWNT	single-walled carbon nanotube
GO	graphene oxide
2D	two-dimensional
NMR	Nuclear Magnetic Resonance
TEGO	thermally expanded graphite oxide
MEGO	microwave-expanded graphite oxide
DMF	dimethylformamide
DCM	dichloromethane
PS	polystyrene
PC	polycarbonate
PMMA	poly(methyl methacrylate)
PVA	poly(vinyl alcohol)
PVC	poly(vinyl chloride)
MMT	montmorillonite
HDPE	high density poly(ethylene)
LDPE	low density poly(ethylene)
EVA	ethylene vinyl acetate
PEN	poly (ethylene-2, 6-naphthalate)
PP	polypropylene
PE	poly (ethylene)
GNP	graphene nanoplatelets
PU	polyurethane
UHMWPE	ultrahigh molecular weight poly(ethylene)
Xc	crystallinity
E	Young's modulus

σ_{max}	tensile strength
ε_{max}	elongation at break
Si_3N_4	silicon nitride
WS_2	inorganic fullerene-like tungsten disulfide
OMMT	organo-montmorillonite
ADA-MONT	acid modified montmorillonite
OTR	oxygen transmission rate
GNF	graphite nanofibre
FTIR	Fourier Transform Infrared Spectroscopy
XRD	X-Ray Diffraction
SEM	Scanning Electron Microscopy
DSC	Differential Scanning Calorimetry
TGA	Thermal Gravimetric Analysis
MFI	Melt Flow Index
d	interlayer spacing(Armstrong)
λ	wavelength
T_m	melting point, ^oC
T_c	crystallization temperature, ^oC
ΔH_m	melting heat (J/g)
ΔH_{100}	melting heat for 100% crystalline nylon-6, 240J/g
W_p	weight fraction of polymer in sample
M_t	weight gained by the nanocomposites
W_d	weight of dry material prior to water immersion
W_w	weight of material after absorbing water

LIST OF APPENDICES

CHAPTER 1

INTRODUCTION

1.1 Background

Polymers are able to offer the advantages of low cost, easy processing, possible recyclability and applicability as sustainable materials as compared to the other types of materials (Wang, Yan and Ma, 2012). They, however, possess much weaker mechanical and thermal properties when put into comparison with specific materials such as metals. The development of polymer nanocomposites(PNCs) as the result of advancement in the area of nanoscience and nanotechnology offers great possibility of high performance materials production for application in a number of areas, resolving issues resulted from the feebleness of polymers (Anandhan and Bandyopadhyay, 2011). A polymer nanocomposite (PNC) is made up of a polymer matrix in which nano-sized additives are incorporated. The nano-sized additives can be of zero-dimensional (nanoparticle), one-dimensional (nanofibres), two-dimensional (graphene sheets) or three-dimensional (spherical particles) (Rafie et al., 2010; Horacio et al., 2011).

The first major success of polymer nanocomposites was reported by Kojima et al. (1993) from the Toyota Central R&D group. They had successfully proved the extraordinary improvement in the thermal and mechanical properties of nylon-6/clay nanocomposites. Since then, PNCs has attracted considerable interest due to infusion of merely small quantity of inorganic nano-scale filler into the polymer matrix leads to prominent enhancement in mechanical, optical, electrical, and thermal properties of the resulted materials as compared to the neat polymers or microfillers composites

(Horacio et al., 2011; Greco, Timo and Maffezzoli, 2012). Typical filler amount of less than 5 wt% brings about effective improvement of the nanocomposite properties due to the large surface area to volume ratio of fillers. (Sangwan, Way and Wu, 2009; Horacio et al., 2011) Although PNCs indicate significantly improved properties, they at the same time retain the desired properties of polymers (Yang et al., 2009).

A very well-known type of polymer nanocomposites is the carbon nanotubes (CNTs)-reinforced composites (Horacio et al., 2011). CNTs had been considered to be an ideal candidate for the reinforcement of polymer composites to enhance the mechanical, electrical, and thermal properties (Kilbride et al., 2002). Figure 1.1 shows a CNT. Zhu et al. (2003) reported for 1wt% loading of functionalized single-walled carbon nanotubes (SWCNTs), the enhancements in modulus and strength in epoxy was 30% and 15% respectively. Unfortunately, the further development of nanocomposites reinforced by CNTs has been obstructed as a result of the prohibitively high cost, allegation against biosafety, blackening of the products and low dispensability of the fillers in the polymer matrix due to their tendency to form bundled agglomerates in the polymer matrices (Horacio et al., 2011; Morimune, Nishino and Goto, 2012).

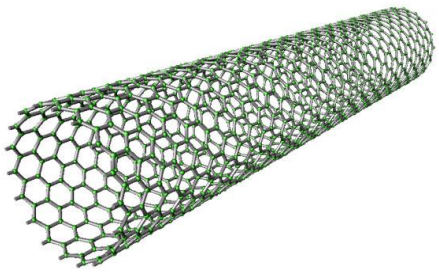

Figure 1.1: Single-walled Carbon Nanotube (CNT) (Cheran, Cheran and Thompson, 2014)

The discovery of graphene has led to the succeeding development of graphene-based polymer nanocomposites. Graphene as illustrated in Figure 1.2 is a 2-dimensional single atomic layer of sp^2 hybridised carbon atoms arranged hexagonally (Horacio et al., 2011; Li et al., 2014). It is also the building block of graphite, CNTs and fullerene which are graphitic carbon allotropes of different dimensionality (Geim

and Novoselov, 2007). The hexagonal ring composed of three in-plane p_z orbitals in the direction normal to the planes that bond the layers of graphene. Due to the weak p_z interaction, delamination can easily take place between the graphene layers under shear stress while the hexagonal structure remains stable (Wang, Yan and Ma, 2012).

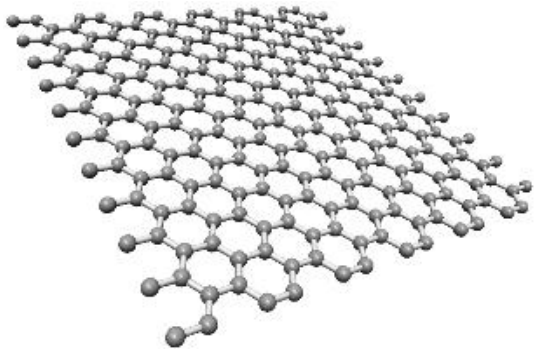

Figure 1.2: Ball-and-stick Representation of the Carbon Atom Arrangement in Graphene (Nanocvd.co.uk, 2015)

Nanoindentation on a free-standing monolayer graphene indicated that it is a material of great stiffness and strength with modulus of approximately 1TPa and strength of 100GPa (Wang, Yan and Ma, 2012; Lee et al., 2008; Scharfenberg et al., 2011). Sheets of graphene have higher surface to volume ratio as compared to CNTs as polymer molecules are incapable to access to the inner surface of the nanotubes. Thus graphene sheets seem to be a more favourable choice for altering mechanical, rheological and permeability properties as well as thermal stability of polymer matrix (Horacio et al., 2011). In fact, Wang, Yan and Ma (2012) also stated that graphene demonstrates electrical, mechanical and thermal properties, specific surface area and aspect ratio superior to the other fillers such as Kevlar fibres.

The improvement in the mechanical properties of graphene-incorporated nanocomposites is also attributed to the better capacity of graphene to deflect crack growth (Rafie et al., 2010). The wrinkled structures given rise by graphene sheets or platelets disseminated in polymer matrix tend to unfold instead of stretch when subjected to stress. This may, to a great extent reduce the stiffness of the material (Wakabayashi et al., 2008). Nevertheless, these structures could result in mechanical interlocking and allows load transfer between polymer matrix and graphene which

could be the reason behind the improved mechanical strength (Srivastava et al., 2011). In addition, graphene can be obtained from natural graphite and results in lower production costs (Horacio et al., 2011).

There has also been growing attention in thermoplastic composites and nanocomposites attributed to the appealing features of thermoplastics in relation to manufacturing cost, environmental compatibility and impact resistance. However, analysis of the effect of nanofillers on thermoplastic matrix is rather complicated owing to the impact of the filler on the crystallization behavior of polymer matrix (Greco, Timo and Maffezzoli, 2012).

1.2 Problem Statements

Polymer nanocomposites with graphene fillers infused have demonstrated their huge potential for several applications such as electronics, aerospace and automotive industries (Wang, Yan and Ma, 2012). As in any nanofillers, the efficient properties enhancement of the host matrix can be only achieved provided that the graphene is homogeneously dispersed in the polymer matrix (Horacio et al., 2011; McAllister et al., 2007). Strong interfacial interactions between graphene and the matrix are also essential to enable the external load to be efficiently transferred through the interactions (McAllister et al., 2007). Nevertheless, the chemically inert property of graphene prevents any kind of interaction with the polymer matrices. The limited groups of polymer which graphene is able to interact efficiently with usually contain aromatic rings. With the purpose of making graphene compatible with wider variety of polymer matrices, the interfacial interactions have to be maximized through chemical modification to introduce other functional groups to the pristine graphene (Horacio et al., 2011).

Graphene oxide (GO) is a derivative of graphene which bears oxygen functional groups on its basal planes and edges. The oxygen-containing functionalities in GO enable it to be well-dispersed in water and several types of polymer matrices (Morimune, Nishino and Goto, 2012) at the same time retains much of the properties

of pure graphene (Marques et al., 2010). Apparently, GO provides a solution to the issue of dispensability of graphene. Additionally, GO is much easier and cheaper to process and produce in bulk quantities (Marques et al., 2010). These characteristics have made GO the more promising filler in manufacturing of polymer nanocomposites.

In this study, GO is incorporated into a thermoplastic polymer, nylon-6 via melt compounding method. The performance of the neat polymer and GO-reinforced polymer is tested and compared in terms of mechanical strength, process ability, physical properties and thermal stability.

1.3 Research Objectives

The aim of this study is to produce nanocomposites with superior mechanical and thermal properties. The specific objectives of this study are:

i) To prepare and characterize graphite oxide.
ii) To prepare and characterize nylon-6/GO nanocomposites.
iii) To test the mechanical, process ability, water absorption and thermal properties of nylon-6/GO nanocomposites.

CHAPTER 2

LITERATURE REVIEW

2.1 Graphene Oxide (GO)

Graphene oxide (GO) is a single atomic layered material derived from exfoliation of graphite oxide (Yang et al., 2009). Graphite oxide can be easily produced by exhaustive oxidation of graphite crystals using strong mineral acids and oxidizing agents (Dreyer et al., 2010). Graphite is made up of layers of graphene aligned in AB stacking sequence. The distance between the layers maintained by van der Waals forces is about 0.34 nm (Ciszewski and Mianowski, 2013). Chemical oxidation of graphite involves intercalation of a wide range of oxygen-containing chemical functionalities in the interlayer space that disrupts the delocalised electronic structure of graphite layers (Potts et al., 2010). This breaks the Van der Waals forces which hold the layers and increase the distance between the layers (Ciszewski and Mianowski, 2013). The oxygenated graphite solids are then hydrolysed and rinsed with water. Solid graphite oxide is recovered by drying. The drying process can be done in atmospheric pressure or vacuum at room temperature. Alternatively, it can be heated in air at low temperatures (50-65^{o}C) to avoid thermal decomposition. Normally, some residual water is present in the solid obtained due to the low drying temperature. Graphite oxide can then be readily exfoliated into GO nanosheets (Li et al., 2014).

Structurally, GO is similar to a graphene sheet. The structure of GO is as shown in Figure 2.1. However compared to graphene, GO contains a range of functional groups containing oxygen for instance hydroxyl and epoxide in the basal planes and carboxyl groups at edges of plane (Sengupta et al., 2011). The GO sheets

consist of both aromatic regions containing unoxidized benzene rings and aliphatic regions with oxidized six-carbon rings where oxygen-containing groups attach to. The carbon-oxygen bonds cause partial change of carbon atoms hybridization from sp^2 to sp^3 which leads to the insulating property of GO (Bykkam et al., 2012). Since the oxygen-containing functional groups have high affinity to water molecules, GO is able to disperse in water and at the same time maintain its suspensibility in organic solvents (Niyogi et al., 2006; Si and Samulski, 2008; Paredes et al., 2008). Stirring and sonication of GO in solvents further enhance the dispersions of graphene oxide fillers (Zhu et al., 2010). Ramanathan et al. (2008) stated that the oxygen-containing groups in GO attribute to better adhesion and improved mechanical interlocking with the polymer chains.

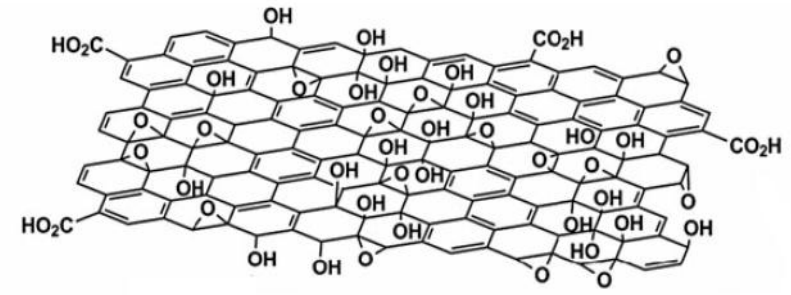

Figure 2.1: Structure of GO (Dreyer et al., 2009)

GO is commonly "reduced" by thermal annealing or chemical reducing agents to partially restore some of the electrical, mechanical as well as thermal properties of the pristine graphene (Raidongia, Tan and Huang, 2014). Several literatures have reported the chemical production of graphene from GO. Redox method is the most popular method to prepare graphene (Park and Ruoff, 2009; Zhu et al., 2010). The oxidation of graphite crystal with strong oxidizing agents is followed by thermal or ultrasonic treatment to remove the functional groups in order to obtain the graphene sheet. This method can give a very high production of graphene and improve the compatibility of matrix composite by introduction of functional groups in the oxidation process.

Indeed, other than making graphene, GO itself exhibits many fascinating properties. It seems to fit into the categories of soft material such as a liquid crystal, membrane, anisotropic colloid, two-dimensional (2D) polymer or amphiphile (Raidongia, Tan and Huang, 2014; Cote, Kim and Huang 2009). Additionally, the functional groups provide active sites for additional chemical modification for instance functionalization (Dreyer et al., 2010).

2.2 Structural Models of GO

Several structural models have been proposed for GO since its discovery by Brodie in 1855. Many earliest structural models suggested that GO was composed of regular lattices with distinct repeat units. Structure proposed by Hofmann and Holst comprised only of epoxy groups scattered on the basal planes of graphite where oxygen is bound to the carbon atoms of the hexagonal layer by epoxide linkages. Figure 2.2 displays Hofmann and Holst's Model. This gives the GO a net molecular formula of C_2O (Hofmann and Holst, 1939). Ruess (1946) who took into account of the hydrogen content of GO, proposed a slightly different model which included hydroxyl groups on the basal plane other than epoxy groups as illustrated in Figure 2.3. This model also indicates that the carbon atoms in the basal plane of GO is sp^3 hybridized rather than the sp^2 hybridized in Hofmann and Holst's model.

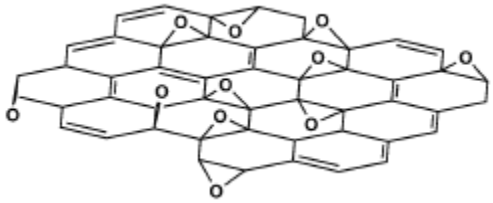

Figure 2.2: Hofmann and Holst's Model (Dreyer et al., 2009)

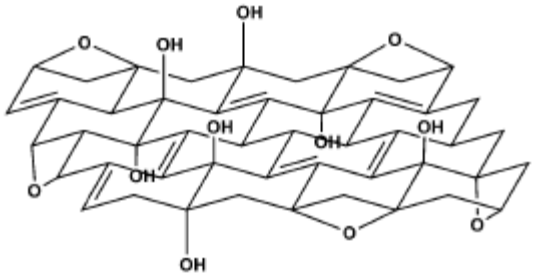

Figure 2.3: Ruess's Model (Dreyer et al., 2009)

Later, Scholz and Boehm (1969) suggested a model which contains neither of the epoxide nor ether groups as provided in Figure 2.4. This model composes of regular quinoidal species and conjugated carbon backbone. Another model by Nakajima and Matsuo (1988) as shown in Figure 2.5 suggested that two carbon layers link to each other by sp^3 C-C bonds perpendicular to the layers. This model stressed on the interactions of the hydroxyl and carbonyl groups between the sheets. They observed the changes in the interlayer spacing in GO with humidity and argued that it can be directly related to the ratio of hydroxyl to carbonyl groups which ranges from a completely dehydrated C_8O_2 to structure dominated by hydroxyl group $C_8(OH)_4$.

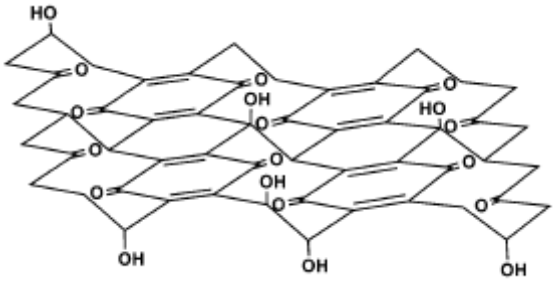

Figure 2.4: Scholz and Boehm's Model (Dreyer et al., 2009)

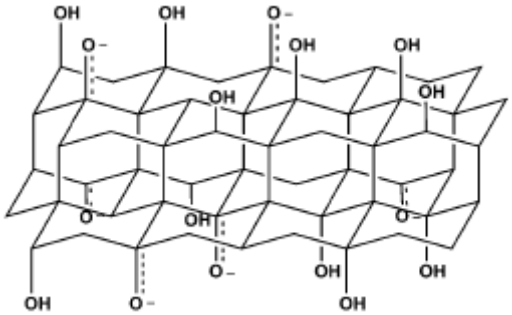

Figure 2.5: Nakajima and Matsuo's Model (Dreyer et al., 2009)

The actual chemical structure of the GO has been under debate due to the complexity of the material and lack of precise characterization techniques (Dreyer et al., 2009). The most well-known model of the recent ones was proposed by Lerf and Klinowski as illustrated in Figure 2.6 although there has been updated structure from Gao et al. (2009). The model is based on the random distribution of aromatic regions of unoxidized benzene rings and regions with aliphatic six-member rings where the oxygen functionalities such as epoxides, carbonyl, carboxyl and hydroxyl groups attach to. Lerf and Klinowski found that epoxy and hydroxyl groups were usually located fairly close to each other by Nuclear Magnetic Resonance (NMR). Modern models and experimental measurements of GO indicate a random distribution of functional groups similar to Lerf and Klinowski model (Raza H, 2012). Observation under high-resolution transmission electron microscopy (HRTEM) supports the Lerf and Klinowski model (Erickson et al., 2010).

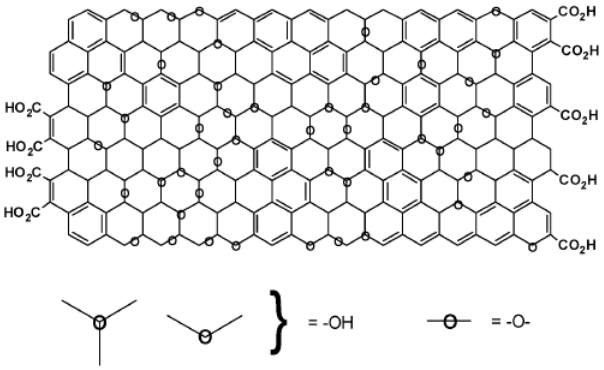

Figure 2.6: Lerf and Klinowski Model of GO (Dreyer et al., 2009)

Regardless of to which model is accurately representing the structure of GO, the presence of oxygen functionalities enables it to interact with hydrophilic polymers as well as aqueous and non-aqueous solvents for wider applications.

2.3 Morphological State of GO in Polymer Matrix

Graphite oxide has a layered structure resembling certain silicates which have been extensively studied as composite fillers (Paul and Robeson, 2008). Previous studies on nanoclay-based composites suggested three common platelet dispersion states namely stacked, intercalated, or exfoliated for layered structure nanofillers as represented in Figure 2.7. In fact, similar dispersion pattern of graphene-based fillers in polymer matrix has been perceived in both graphene nanoplatelets (GNP) and GO-based polymer nanocomposites (Potts et al., 2010).

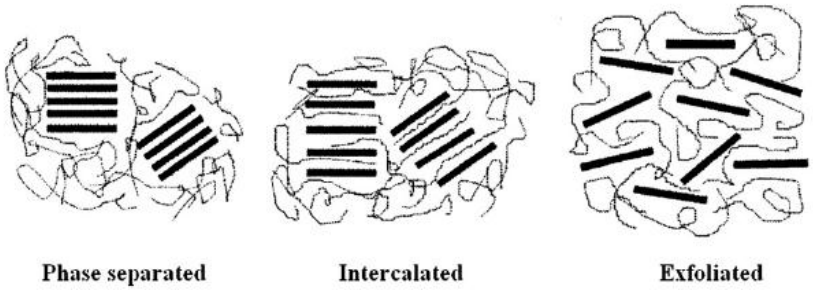

Figure 2.7: Morphological States of Graphene-based Nanocomposites (Wang, Yan and Ma, 2012).

To enhance the properties of GO/polymer nanocomposites effectively, graphite oxide has to be exfoliated so that the graphene oxide sheets are well dispersed in the polymer matrix (Thostenson, Li and Chou, 2005). An exfoliated graphite oxide has a higher aspect ratio in contrast to either intercalated or stacked state (Fu and Qutubuddin, 2001).

2.4 Preparation of GO

The preparation of GO involves two basic steps where graphite powder is oxidized to graphite oxide and followed by exfoliation of graphite oxide into graphene oxide (GO). Figure 2.8 demonstrates the steps in preparing GO.

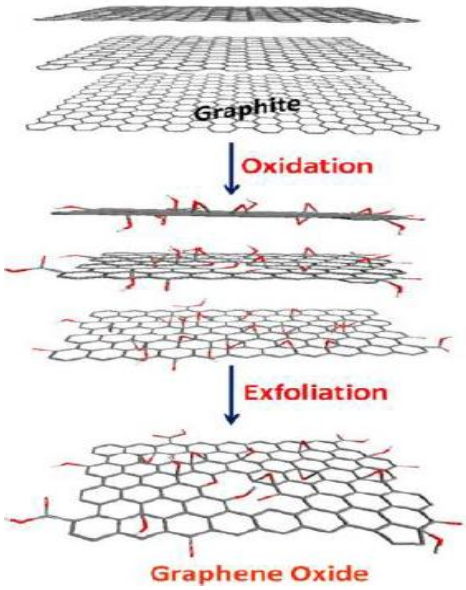

Figure 2.8: Steps in Preparing GO (Su and Loh, 2012)

2.4.1 Synthesis of Graphite Oxide

In year 1859, a British chemist, Brodie produced the very first graphite oxide through addition of potassium chlorate ($KClO_3$) to graphite slurry in fuming nitric acid (HNO_3). The overall mass of the material formed was found to increase due to its carbon, hydrogen and oxygen composition rather than carbon alone in graphite. The oxidation was repeated for another three times until the oxygen content reached the maximum. The net molecular formula obtained was $C_{2.19}H_{0.80}O_{1.00}$.

Nearly 40 later, L. Staudenmaier (1898) slightly improved Brodie's method by dividing the chlorate to multiple portions and adding them one after another. Concentrated sulfuric acid was also added to increase the acidity of the mixture.

Similar overall extent of oxidation was achieved as in Brodie's approach where the ratio of carbon and oxygen of 2 to 1.

Nitric acid and potassium chlorate are strong oxidizing agents which react strongly with aromatic carbons (Lakshminarayanan et al., 2004; Zhang et al., 2008; Dreyer et al., 2009). Potassium chlorate is commonly used in explosive materials (Dreyer et al., 2009). The oxidation processes involving potassium chlorate are vigorous which may result in spontaneous ignition or explosion (Wu & Ting, 2013).

Afterwards, Hummers and Offeman(1958) oxidized graphite through an alternative means using concentrated sulfuric acid (H_2SO_4) and potassium permanganate ($KMnO_4$) as oxidizing agents. This method also includes the use of sodium nitrate. After oxidation step, hydrogen peroxide is added to the diluted mixture to reduce the manganese. In this method, the active species in permanganate is diamanganese heptoxide (Mn_2O_7). The formation of diamanganese heptoxide from potassium permanganate is shown in Figure 2.9.

$$KMnO_4 + 3H_2SO_4 \rightarrow K^+ + MnO_3^+ + H_3O^+ + 3HSO_4^-$$
$$MnO_3^+ + MnO_4^- \rightarrow Mn_2O_7$$

Figure 2.9: Formation of Diamanganese Heptoxide (Mn_2O_7) from Potassium Permanganate ($KMnO_4$) in the Presence of Strong Acid (Dreyer et al., 2009)

These three reactions achieve similar levels of oxidation where ratio of carbon to oxygen is approximately 2:1 (Dreyer et al., 2010). Comparatively, Hummers method takes the shortest time to produce GO (Ciszewski and Mianowski, 2013). Other than that, it is less hazardous then the other two methods. In spite of slightly modified versions developed over the years, these three methods comprise the primary routes for producing GO.

2.4.2 Exfoliation of Graphite Oxide

Solvent exfoliation and thermal exfoliation have arisen as two common techniques for exfoliation of graphite oxide. In solvent exfoliation, graphite oxide is exfoliated by ultrasonication or mechanical stirring in water or polar organic solvents. This form colloidal suspensions of GO (Potts et al., 2011). Sonication process may lead to fragmentation of the platelets and reduction of their lateral dimensions. Mechanical stirring is able to produce GO platelets of larger lateral dimensions but in a very slow way along with low yield (Dryer et al., 2010).

Alternatively, graphite oxide can also be exfoliated by heating rapidly. This produces thermally expanded graphite oxide (TEGO). This method involves charging of the dry graphite oxide powder into a vessel such as quartz tube and subjecting to thermal shock. The rapid heating causes small molecules such as carbon dioxide and water to escape and force the sheets to be apart from each layer (McAllister et al., 2007). Microwave radiation is also capable of exfoliating GO to produce microwave-expanded graphite oxide (MEGO) (Zhu et al., 2010). Interestingly, these processes reduce GO at the same time exfoliating it.

2.5 Fabrication of Polymer Nanocomposites

There are generally three methods used to produce polymer matrix nanocomposites namely in situ polymerization, melt blending or solution blending. These methods are also able to disperse the filler in polymers (Wang, Yan and Ma, 2012). Table 2.1 summarizes some examples of the polymer nanocomposites fabricated via these methods.

2.5.1 Solution Blending

Solution blending is the most popular fabrication technique of polymer composites. It takes advantage of the good solubility of polymer in usual organic and aqueous solvents such as chloroform, acetone, toluene, dichloromethane (DCM), dimethylformamide (DMF) and water. The polymer is solubilized in a solvent and followed by mixing with dispersed suspension of filler (Wang, Yan and Ma, 2012). The resulting suspension is then precipitated using a non-solvent of the polymer. The precipitate can then be dried and further processed. Alternatively, the suspension can be cast into a mold and remove the solvent. However, the latter may lead to filler aggregation in the composite (Potts et al., 2011).

GO has previously been successfully infused to some polymers including poly(methyl methacrylate) (PMMA), polycarbonate (PC), polystyrene (PS), polyimides and polyacrylamide using this technique. In the fabrication of the reported nanocomposites, GO surface was usually functionalized using isocyanates, alkyl-chlorosilanes and alkylamine to make it more dispensable in organic solvents (Stankovich et al., 2006; Ramanathan et al., 2008; Higginbotham et al., 2009; Chen, Zhu and Liu, 2010). In this case, aqueous GO suspensions can also be produced via sonication prior to mixing with water-soluble polymers such as poly(allylamine) and poly(vinyl alcohol) (PVA) (Xu et al., 2009).

2.5.2 Melt mixing

This technique utilizes elevated temperature to turn the polymer into molten phase and shear to intercalate fillers in polymer matrix. The benefit of using this technique is the elimination of the use of toxic solvents (Wang, Yan and Ma, 2012). This technique is believed to be more cost effective than solution blending and is more compatible with industrial processes. Furthermore, it is said to be more environmentally friendly due to elimination of solvent use, faster and easier (Naffakh et al., 2011). However, such methods may not be able to achieve same level of filler dispersion as solvent mixing or in situ polymerization methods at high filler loadings

(Potts et al., 2011). Examples of nanocomposites fabricated by this method include polypropylene (PP)/GNP, high density poly(ethylene) (HDPE)/ nanoclay, PMMA/glass flake, nylon-11/graphene and nylon-12/graphene (Cunha et al., 2015; Tanasa and Zanoaga, 2014; Salehi, Ehsani and Khonakdar, 2015; Rafiq et al., 2013).

2.5.3 In situ polymerization

For this method, the filler is mingled in neat or multiple monomers to intercalate the monomers between layers of filler. Polymerization is carried out subsequently to separate the layers. The nanocomposite is subsequently produced through precipitation or solution casting. This method is capable of producing composites with covalent linkage between the filler and the polymer matrix. Unlike the other two methods, this method is capable in achieving high level of dispersion of filler without prior exfoliation step (Wang, Yan and Ma, 2012). For instance, nanocomposites such as polyamide-6/GO, polyimide/GO, Nylon-6/ADA-MONT have been developed through in situ polymerization.

Table 2.1: Examples of Polymer Nanocomposites Fabricated through Different Methods

Fabrication method	Polymer	Reference
Solution Blending	PVC/MMT	Madaleno, Schjødt-Thomsen and Pinto, 2010
	HDPE/Nanoclay	Tanasa and Zanoaga, 2014
	LDPE/EVA/Graphene	Tayebi et al., 2015
	PVA/Graphene	Wang, Wu and Qian,2015
	PMMA/GO	Ramanathan et al., 2008
	PC/GO	Higginbotham et al., 2009
	PS/GO	Stankovich et al., 2006
	Polyimide/GO	Chen, Zhu and Liu, 2010
	Polyacrylamide/GO	Chen, Zhu and Liu, 2010
	Epoxy/GO	Yang et al., 2009

Melt Mixing	PP/GNP	Cunha et al., 2015
	HDPE/Nanoclay	Tanasa and Zanoaga, 2014
	PMMA/Glass flake	Salehi, Ehsani and Khonakdar, 2015
	Nylon-11/Graphene	Rafiq et al., 2013
	Nylon-12/Graphene	Rafiq et al., 2013
In situ Polymerization	Polyamide-6/GO	Zhang et al., 2012
	Polyamide-6/GO	O'Neill, Bakirtzis and Dixon, 2014
	Polyimide/GO	Hu et al., 2011
	Nylon-6/ADA-MONT	Liang et al., 2008

2.6 GO/Polymer Nanocomposites

It has been reported that the properties of many polymers such as PVA, PU (polyurethane), epoxy, PC, PMMA, PS have been successfully improved by incorporation of GO (Xu et al.,2009; Nguyen et al., 2009; Fang et al., 2009; Fang et al., 2010; Kim and Maacosko, 2009; Goncalves et al., 2010; Xu and Gao, 2010). Yang et al. (2009) reported that GO/epoxy nanocomposite prepared by solution blending indicated significant improvements in mechanical properties with an increase of 48.3% in compressive failure strength and 1185.2% in toughness respectively when 0.0375wt% of GO is used. The authors regarded the significant effect of the low loading of GO on epoxy as the result of wrinkled topology at the nanoscale. Other than the strengthened mechanical interlocking between filler and polymer chains and better adhesion caused by the nanoscale surface roughness, GO contains oxygen functionalities across its surfaces which may contribute to the formation of covalent bonds with functional groups in epoxy. The large surface area of GO sheets further promoted the strong interfacial interactions with epoxy resin (Yang et al., 2009).

Morimune, Nishino and Goto (2012) prepared graphene oxide reinforced PVA by using simple casting method from aqueous medium. The Young's modulus (*E*) of PVA increased dramatically for 76% at low GO loading of 0.1wt%. The stress-strain

curve is indicated by Figure 2.10. The authors concluded that GO bound strongly with PVA by hydrogen bonding. At low GO loading, slippage of graphene sheets during the tensile testing suppresses the rapid decreasing of the ε_{max}. As the content of GO in the PVA matrix was further increased, the interactions between GO sheets particularly Van der Waals force caused formation of agglomerates by stacking the sheets together and thus cause brittle failure.

Thermogravimetric traces under nitrogen flow also showed that the onset temperature for thermal degradation of the PVA/GO nanocomposite with 1wt% GO content was about 10 ℃ higher than that of the PVA film as shown in Figure 2.10. Nano dispersed of GO acts as a barrier to prevent the volatile decomposition products from diffusing out of the composites with its plate-like configuration, thus decreasing the permeability of PVA/GO nanocomposites.

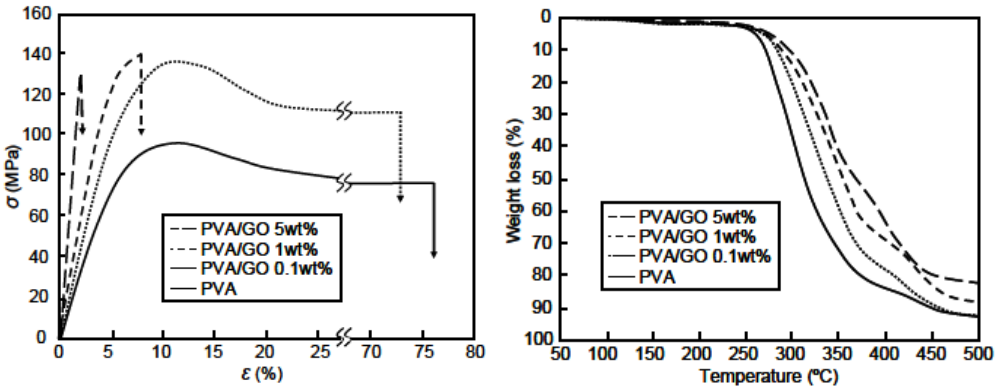

Figure 2.10: (a) Stress-strain Curve (b) Thermogravimetric Traces of GO/PVA Nanocomposites (Morimune, Nishino and Goto, 2012)

Figure 2.11 presents the swelling ratio of the PVA/GO nanocomposites placed in distilled water at 30 ℃. The swelling was suppressed by the presence of GO where the swelling ratio decreased by more than 50% for all nanocomposites. The dispersion of high aspect ratio GO sheets had lengthened the penetration path of water in the PVA matrix.

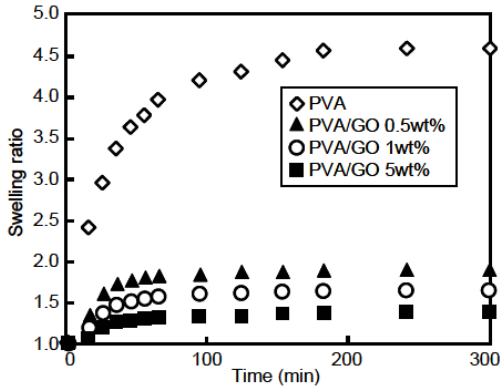

Figure 2.11: Swelling Ratio of PVA/GO Nanocomposites in Distilled Water at 30 ℃ (Morimune, Nishino and Goto, 2012)

The mechanical properties of PU infused with GO by solution blending was investigated by Pokharel, Choi and Lee (2014). Two different PU of varied segmental length were involved in the study, namely S-PU and L-PU. As shown in Figure 2.12, both of the PU exhibited greater tensile strength and Young's modulus with increasing GO content due to the effective load transfer between the filler and the polymer matrix. Increased GO loading also boosted the strain-induced hardening effect due to urethane linkage and secondary bonding.

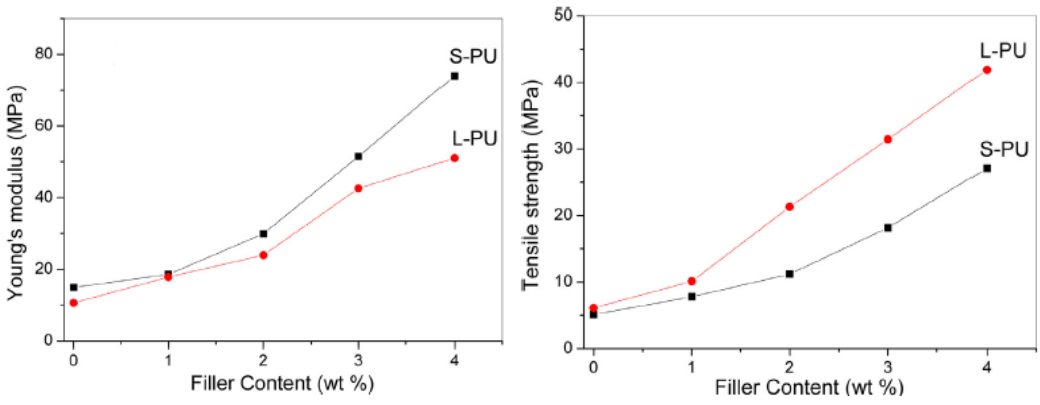

(a) (b)

Figure 2.12: (a) Young's Modulus and (b) Tensile Strength of GO/PU Nanocomposites (Pokharel, Choi and Lee, 2014)

Suner et al. (2015) had carried out a study on the thermal and mechanical properties of ultrahigh molecular weight poly(ethylene) (UHMWPE) prepared by solution mixing. It was found that the Young's modulus, yield stress improved for approximately 15% while fracture strength enhanced for 25% with addition of up to 0.5wt% of GO. A downward trend was observed in these properties with further addition of GO. On the other hand, TGA stipulated that the oxidation temperature, linear weight loss stage, end of linear weight loss and complete volatilization temperature shifted to higher temperatures.

However, GO-reinforced polyimide fabricated via in situ polymerization by Hu et al. (2011) indicated a different behavior that the modulus did not increase distinctly until the concentration of GO in polyimide reached 10% by weight. The authors stated that neat polyimide possesses excellent mechanical properties with high modulus that it can barely be further enhanced with low concentration of GO. Moreover, the increment in elongation at break could only be observed at addition of 10wt% GO, indicating load transfer across the GO sheets-matrix interface. Nonetheless, the strength of the composite film was lower than the base polymer at this concentration of GO. Additionally, the thermal degradation behavior of the GO/polyimide nanocomposites suggested that the addition of GO did not enhance the thermal stability of polyimide. The mechanical and thermal properties of GO/polyimide are shown in Table 2.2 and Figure 2.13.

Table 2.2: Mechanical Properties of Polyimide and GO/Polyimide Nanocomposites (Hu et al., 2011)

GO sheets (wt%)	Modulus (GPa)	Strength (MPa)	Elong@break (%)
0	2.2±0.3	129±4	13±2
0.5	2.3±0.2	125±3	12±1
1	2.8±0.2	136±5	10±2
10	4.1±0.4	92±8	25±5

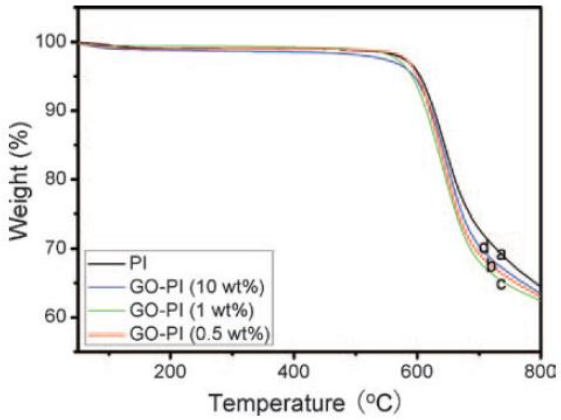

Figure 2.13: TGA Traces of GO/Polyimide Nanocomposites of Different GO Concentration (Hu et al., 2011)

2.7 Nylon-6

Nylon is a widely used thermoplastic polymer due to its corrosion resistance, good insulation and good load bearing capacity. On top of that, it has low density which makes it lighter. For a specific volume, nylon comprises of roughly one-eight of the weight of bronze, 14.3% of the weight of cast iron and half of the weight of aluminum (Rangari et al., 2008).

Nylon-6, or polycaprolactam is synthesized through ring-opening polymerization of a cyclic amide namely caprolactam as displayed in Figure 2.14. The name of nylon-6 comes from the 6 carbons in caprolactam. To form the polymer, the amide bond within each caprolactam molecule breaks and re-forms two new bonds with other monomers.

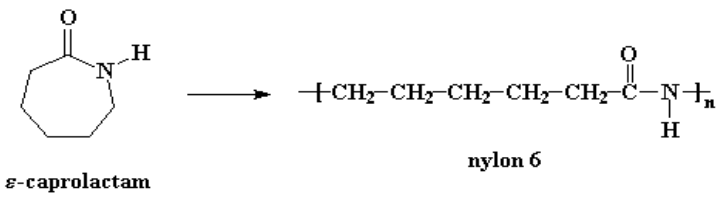

Figure 2.14: Formation of Nylon-6 from Caprolactam (Phlegm, 2009)

Nylon-6 is a tough material which is abrasion-resistant. In contrast to the more common nylon-6/6, it has improved surface appearance, processability and creep resistance (RTP Co., 2014). Due to its lower crystallinity, it can be molded at lower temperature with less mold shrinkage. Adversely, nylon-6 has a lower modulus and higher absorption rate of moisture than nylon-6/6. Moisture is able to reduce the tensile strength and stiffness while increasing elongation as plasticizer does. Although moisture absorption confers many undesirable changes in properties, impact strength and general energy absorbing characteristics of nylon increases prominently as moisture content rises. Nylon-6 is used in applications such as gear wheels where toughness, lubricity and wear are important.

In the early 1990, Toyota has developed nylon-6/clay hybrid to fabricate automotive timing belt cover. It was the very first time a polymer nanocomposite was applied in engine part. In the hybridization process by the Toyota, sodium montmorillonite is mixed with α, ω-amino acid in hydrochloric acid to protonate the amino acid. The amino acids then exchange with the sodium counterions. As a result, the alkyl units of the organoclay contain terminal carboxyl groups which play the role of initiating ring-opening polymerization of caprolactam, forming nylon-6 chains bonded ionically to the aluminosilicate platelets as demonstrated in Figure 2.15 (Fornes and Paul, 2003).

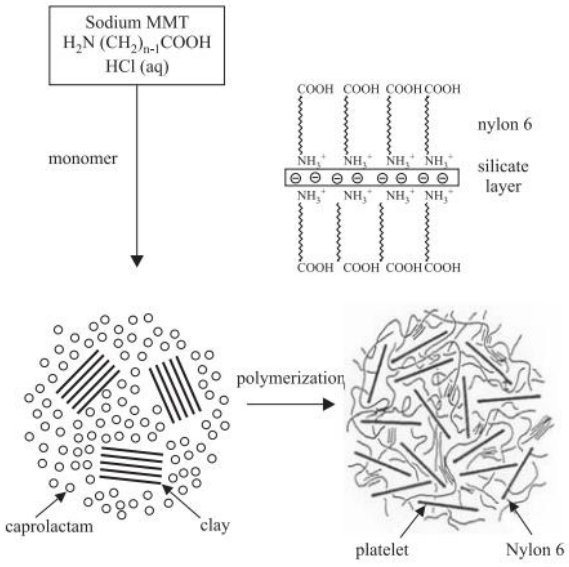

Figure 2.15: Formation of Nylon-6/Clay Hybrid by In Situ Polymerization (Toyota Process) (Fornes and Paul, 2003)

Nylon-6 clay nanocomposites have high deflection temperature, great stiffness and light weight. For these reasons, they are widely used in automotive industry in under-the hood application and components of fuel system until today (Pandey et al., 2014).

2.8 Nylon-6 Nanocomposites

In studying the properties of nylon-6 nanocomposites, Rangari et al. (2008) infused Si_3N_4 (Silicon nitride) of two different geometries (nanorods and spheres) in nylon-6 via melt processing. They found that the tensile strength and modulus increased for 179.03% and 276.40% respectively as tabulated in Table 2.3. This was attributed to the unusually high load bearing capability of Si_3N_4 nanoparticles and the alignment of filler in the direction of extrusion of nylon-6 polymer filaments during processing.

Table 2.3: Tensile Properties of Nylon-6 and Si_3N_4/Nylon-6 Nanocomposites (Rangari et al., 2008)

Type	Tensile Strength(MPa)	% Improvement	Tensile Modulus	Gain/Loss in Modulus (%)
Neat Nylon-6	248.6 ±16	-	0.6	-
1% Spherical Si_3N_4 + Nylon-6	445.1 ±44	179.03	1.5	272.7
1% Rod Si_3N_4 + Nylon-6	687.3 ±29	276.40	3.4	610.9

Allafi and Pascal (2013) investigated the thermal property of nylon-6/nanoclay nanocomposites fabricated by melt compounding via Dynamic Mechanical Analysis (DMA). The storage modulus of the nanocomposites indicated a prominent improvement as stipulated in Figure 2.16. This was due to the reinforcing effect of the high aspect ratio nanoclay particles and great extent of stress transfer at

the polymer-filler interface. The improvement in the property might also be attributed to hindered segmental motion at the filler-polymer interface.

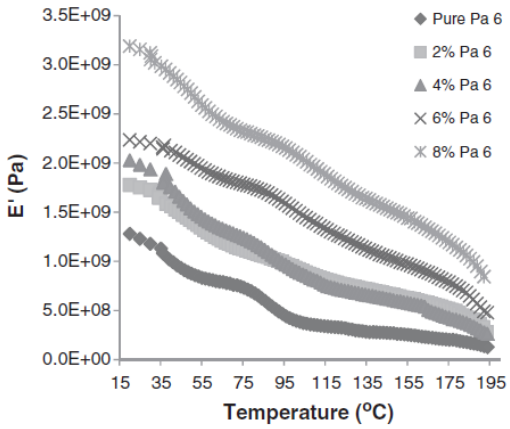

Figure 2.16: Storage Modulus for Nylon-6 and Nylon-6/Nanocomposites Heating at 5 ℃/Min (Allafi and Pascal, 2013)

Another type of nylon-6 nanocomposites was developed by incorporating inorganic fullerene-like tungsten disulfide (WS_2) into nylon-6 via melt mixing. The study was done by Naffakh et al. (2011). Figure 2.17 shows the TGA traces of nylon-6/WS_2. The onset temperature of decomposition shifted by 35^{o}C with addition of merely 0.1wt% of WS_2, signifying a remarkable improvement in thermal stability.

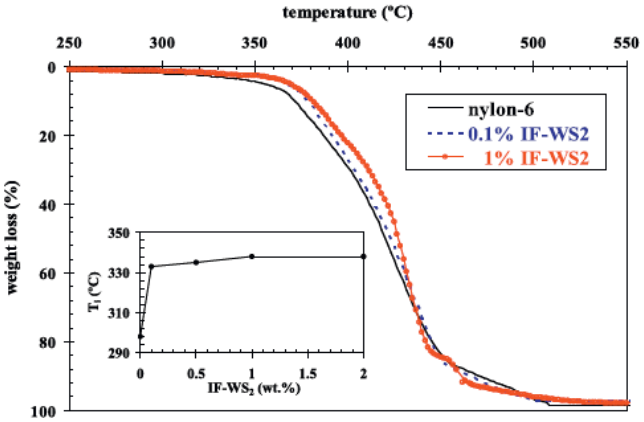

Figure 2.17: TGA Traces of Nylon-6/WS_2 Nanocomposites at heating rate of 20^{o}C/min in oxygen atmosphere (Naffakh et al., 2011)

Hassani, Ishak and Mohamed (2014) had attempted in producing nanocomposites comprised of nylon-6 and commercial CNT as filler via melt compounding. The melt flow rate started to reduce significantly at 1wt% of CNT loadings due to the non-polar nature of CNT which facilitates the movement of polymer chains by acting as barrier to polar-polar interaction in nylon-6. This may ease the processing but at the same time cause unfavorable change in the mechanical properties. The tensile strength of the nylon-6/CNT nanocomposite decreased by 21MPa at 3.0wt% of CNT content as tabulated in Table 2.4.

Table 2.4: MFI and Mechanical Properties of Nylon-6/CNT Nanocomposites (Hassani, Ishak and Mohamed, 2014)

CNT Loadings (wt%)	MFI (g/10min)	Tensile Strength(MPa)	Elongation at Break (%)
0	23.9 ±0.9	75 ±1	28.5 ±12.1
0.1	24.4 ±0.4	63 ±7	5.7 ±2.6
0.2	25.0 ±1.7	69 ±5	9.2 ±5.5
0.5	25.0 ±0.7	67 ±8	6.4 ±3.4
1.0	21.5 ±1.1.5	64 ±14	5.8 ±5.3
2.0	19.8 ±1.1	65 ±15	4.1 ±1.4
3.0	14.6 ±3.3	54 ±10	2.8 ±0.4

Chow and Ishak (2007) reported 30.4% and 71.3% of improvement in the tensile modulus and tensile strength respectively in nylon-6 infused with 4wt% of organo-montmorillonite (OMMT) through melt mixing. At the meantime, the nanocomposite exhibited 38.1% and 11.8% increment in flexural modulus and flexural strength correspondingly. The mechanical properties are summarized in Table 2.5.

Table 2.5: Mechanical Properties of Nylon-6/OMMT Nanocomposites (Chow and Ishak, 2007)

Properties	Unit	PA6	PA6/OMMT
Tensile modulus	GPa	2.3 ± 0.02	3.0 ± 0.02
Tensile strength	MPa	40.1 ± 0.05	68.7 ± 0.10
Elongation at break	%	58.4 ± 0.05	3.5 ± 0.02
Flexural modulus	GPa	2.1 ± 0.02	2.9 ± 0.01
Flexural strength	MPa	94.2 ± 0.10	105.3 ± 0.10

12-Aminododecanoic acid modified montmorillonite (ADA-MONT)/nylon-6 nanocomposites were produced via in situ polymerization by Liang et al. (2001). 116% and 115% increase in flexural modulus and tensile modulus respectively were reported at 8wt% loading of filler as presented in Table 2.6. In addition, the oxygen transmission rate (OTR) was reduced by 80%, stipulating better barrier property of the nanocomposites.

Table 2.6: Mechanical Properties of Nylon-6/ADA-MONT Nanocomposites (Liang et al., 2001)

Nanoclay ADA-MONT (wt. %)	Flexural Modulus (MPa)	Tensile Modulus (MPa)
0%	2836	2961
2%	4326 (53%)	4403 (49%)
4%	4578 (61%)	4897 (65%)
6%	5388 (90%)	5875 (98%)
8%	6127 (116%)	6370 (115%)

As discussed earlier, nylon-6 is known to be hygroscopic that it absorbs water easily. Abacha et al. (2009) carried out a study on the water diffusion behaviour of nylon-6/organoclay nanocomposites prepared by melt mixing method at 40^{o}C, 50^{o}C and 60^{o}C. The highest reduction in water absorbing ability was demonstrated by the nanocomposite containing 2wt% clay as tabulated in Table 2.7. Higher clay

content increased the equilibrium weight as a result of the hydrophilicity of the clay which tends to attract water.

Table 2.7: Maximum Equilibrium Weight Gain (M_∞) of Nylon-6/Organoclay Nanocomposites at 40°C, 50°C and 60°C (Abacha et al., 2009)

Formulation (wt%)	M_∞ (%)		
	40°C	50°C	60°C
0	9.5474	9.3563	9.0050
2	8.2592	8.4331	8.1520
4	8.7598	8.7286	8.4018
6	8.8769	8.6723	8.6060
8	9.5649	9.2829	9.0006

In the present, there has not been much research done on nylon-6/GO nanocomposites. Zhang et al. (2012) reported GO reinforced polyamide-6 nanocomposites fabricated via in situ ring-opening polymerization with significant improvement in tensile strength and Young's modulus at low GO contents. O'Neill, Bakirtzis and Dixon (2014) studied on the thermal properties of polyamide-6/GO nanocomposites produced also via in situ ring opening polymerization. In this study, we are interested to investigate processing, thermal, water absorption and mechanical properties of GO/polyamide 6 nanocomposites fabricated by melt mixing method which is claimed to be more environmentally friendly due to elimination of solvent use, cost effective, faster, easier and applicable in large-scale production (Naffakh et al., 2011).

CHAPTER 3

METHODOLOGY

3.1 Materials

Graphite oxide was prepared from graphite nanofibre(GNF). GNF was supplied by Platinum Senawang Sdn Bhd. Sulphuric acid(H_2SO_4, 95-97%) and hydrochloric acid (HCl, 37%) were provided by QRëC® Sdn Bhd while hydrogen peroxide (H_2O_2, 30-31%) was purchased from SYSTERM® ChemAR®. Potassium Permanganate ($KMnO_4$, 99%) was obtained from Bendosen Laboratory Chemicals and sodium nitrate ($NaNO_3$, 99%) was supplied by GENE Chem.

For the polymer, nylon-6 (polycaprolactam, 3mm pellets, ρ=1.084g/ml) pellets were supplied by Sigma Aldrich. Anodisc membrane used for filtration was bought from Whatman Inc.

3.2 Synthesis of Graphite Oxide

Graphite oxide was produced using the conventional Hummers method. A 500ml beaker filled with 115ml of H_2SO_4 was put under an overhead stirrer for stirring at 400rpm. Ice bath was used to maintain the temperature of the content in the beaker at 0^oC. Then, 5g of Graphite nanofibre (GNF) followed by 2.5g of $NaNO_3$was added into the beaker. After $NaNO_3$ was dissolved, 15g of $KMnO_4$ was added slowly to maintain the temperature below 30^oC. Figure 3.1 shows the experimental setup.

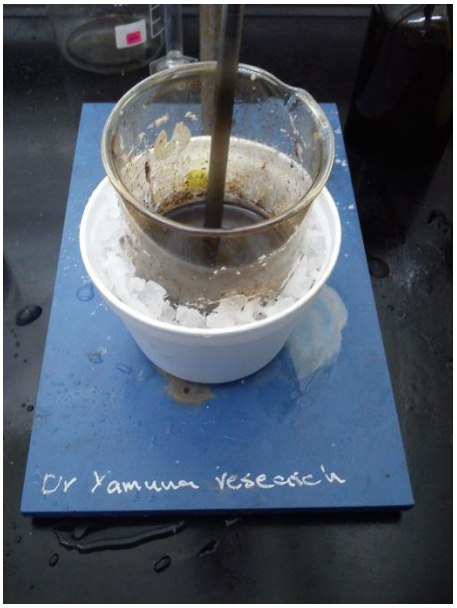

Figure 3.1: Experimental Setup for Graphite Oxide Synthesis

After stirring for 10 minutes, ice bath was removed. The solution was then stirred at 500rpm for 3hours at ambient temperature. After 3 hours, the speed was reduced to 400rpm and 230ml of deionized water was added slowly to the solution. The solution was continued to be stirred for 10 minutes. Then, the solution was poured into 700ml of deionized water. 12ml of H_2O_2 was added to reduce the residual $KMnO_4$. The mixture was left overnight. A dark brown paste settled to the bottom shown in Figure 3.2. The mixture was then filtered using Anodisc membrane.

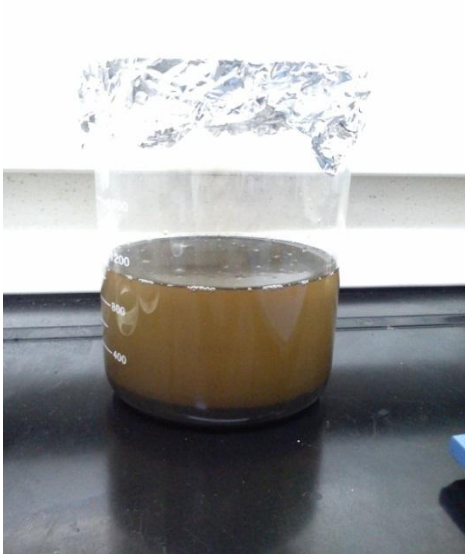

Figure 3.2: Dark Brown Paste Settled to the Bottom after Leaving Overnight

The filtered cake was washed with 5% HCl solution, followed by filtration with Anodisc membrane and washing with deionized water. The solution was centrifuged for 20 minutes at the speed of 10,000rpm. The supernatant was decanted after measuring its pH. Filtration, washing and centrifugation were repeated until the pH of supernatant fell into the range of 5-7. The precipitate was dispersed in deionized water and dried in oven overnight at 60^{o}C.

3.3 Preparation of Nylon-6/GO Nanocomposite Sheets

The nylon-6 pellets were pre-dried in vacuum oven for 24 hours at 80^{o}C to remove any moisture. The nanocomposites were produced by melt mixing method in the Brabender® Plastograph® EC 815652 internal mixer as show in Figure 3.3. 40g of nylon-6 pellets was premixed with graphite oxide and loaded into the mixer operating at 235^{o}C, with rotor rotating at a speed of 60rpm. Mixing was allowed to take place for 7.5 minutes until the polymer and fillers were homogenously mixed. The torque during compounding was recorded. The loadings of GO were 0.5, 1.0, 1.5 and 2.0wt% as tabulated in Table 3.1.

Figure 3.3: Brabender® Plastograph® EC 815652 Internal Mixer

The nylon-6/GO sheets were fabricated using hydraulic hot and cold press machine model GT-7014-A30C as shown in Figure 3.4. The pressing temperature was set to 260^{o}C. The lumps of nanocomposite were preheated for 10 minutes and pressed for 5 minutes. Then, cooling was proceeded for 2 minutes.

Figure 3.4: Hydraulic Hot and Cold Press Machine

Table 3.1: Weight of Nylon-6 and Graphite Oxide for Compounding

Weight Percentage of GO (wt%)	Weight of Nylon-6 (g)	Weight of Graphite Oxide (g)
0	40	0
0.5	40	0.2
1.0	40	0.4
1.5	40	0.6
2.0	40	0.8

3.4 Characterization

3.4.1 Fourier Transform Infrared Spectroscopy (FTIR)

FTIR was carried out using PerkinElmer Spectrum ex1 to identify the types of chemical bonds and functional groups in GNF, graphite oxide and nylon-6/GO nanocomposites. The analysis was carried out to determine the absorption band at the wavelength between 4000cm^{-1} to 400cm^{-1} with 4 scans at a resolution of 4cm^{-1}. For GNF and graphite oxide, the samples are prepared with KBr. For the nanocomposites, very thin films were prepared by hydraulic hot and cold press machine to ensure the penetration of infrared rays. Background spectrum was captured before samples were scanned.

3.4.2 X-Ray Photoelectron Spectroscopy (XPS)

To confirm the FTIR results, XPS was employed to determine the chemical environment of atoms in analyzing the structure of GNF and graphite oxide. The XPS data was taken on ULVAC-PHI Quantera II equipped with monochromatic Al Kα (hν = 1486.6 eV) X-ray source at room temperature.

3.4.3 Raman Spectroscopy

Raman spectra of GNF and graphite oxide were recorded on NT-MDT NTEGRA with 473nm laser excitation of power 1.7mW focused through 100X objective lens to obtain the structural information of the samples. All powder samples were directly deposited on the glass slide in the absence of solvents.

3.4.4 X-Ray Diffraction (XRD)

XRD analysis was run in Siemens XRD Diffractometer 5000 to understand the interlayer spacing and crystalline structure of GNF, graphite oxide and nylon-6/GO nanocomposites using Nickel filtered Copper Kα radiation with λ =0.154nm. The samples were scanned with rate of 1^{o}/min between 0-80^{o}C.

The interlayer spacing was calculated by Bragg's Equation in Equation 3.1:

$$d= \frac{n\lambda}{2sin\theta} \quad (3.1)$$

where
d= interlayer spacing (Armstrong)
λ= wavelength

3.4.5 Morphology Study

Morphology of the GNF and graphite oxide at magnification of X10,000 was examined using Field Emission Scanning Electron Microscopy (FESEM) at accelerating voltage of 2kV. Prior to scanning, the samples were placed on a disc and held in place using a double-sided carbon tape. The samples were then coated with platinum particles to avoid sample charging. The model of equipment used was JOEL JSM 6701F.

3.4.6 Thermal Properties of the Nanocomposites

Mettler Toledo TOPEM was used for determining the melting points, crystallinity and crystallising temperatures of the nylon-6 and nylon-6/GO nanocomposites. For nylon-6, a pellet of the polymer was placed in a 40 μL crucible. For nanocomposites, a small

section of each nanocomposite was cut and placed into the crucible. The weight of the sample was recorded. Then, the crucible was encapsulated with lid. The sample was heated from 25^{o}C to 300^{o}C at a rate of 10^{o}C/min under nitrogen flow of 10ml/min. This was immediately followed by cooling back to 25^{o}C.

The crystallinity is calculated from Equation 3.2:

$$X^{m}_{c} = \frac{\Delta H_m}{W_p \, x \, \Delta H_{100}} \, x \, 100\% \qquad (3.2)$$

where

X^{m}_{c} = crytallinity(%)

ΔH_m = Melting heat (J/g)

ΔH_{100} = Melting heat for 100% crystalline nylon-6, 240J/g

W_p = Weight fraction of polymer in sample

3.4.7 Thermal Decomposition Study

Thermal Gravimetric Analysis (TGA) was performed to determine the decomposition temperature and thus the thermal stability of GNF, graphite oxide and nylon-6/GO nanocomposites. Measurements were carried out under a nitrogen atmosphere at a heating rate from 0^{o} to 750^{o}C using Mettler Toledo TGA SDTA851 E.

3.4.8 Melt Flow Index (MFI)

MFI was done with the purpose of measuring the ease of flow or melt flow rate (MFR) for nylon-6 and nylon-6/GO nanocomposites in molten state. In the testing, Procedure A of ASTM D1238 was applied. The melt flow apparatus used was Tinius Olsen Extrusion Plastometer model MP600 as shown in Figure 3.5. The total mass of material that was extruded from the die was weighted and calculated in g/10min.

Figure 3.5: Tinius Olsen Extrusion Plastometer model MP600

3.5 Performance Test

3.5.1 Tensile Test

Tensile test was carried out according to ASTM D638 under ambient condition to measure the elastic modulus, ultimate tensile strength and elongation at break of nylon-6 and nylon-6/GO nanocomposites. Prior to testing, test specimens as displayed in Figure 3.6 were cut using dumbell press cutter. The test was conducted using Tinius Olsen H10KS-0748 as shown in Figure 3.7 with a load cell of 500N, at a crosshead speed of 50 mm/min. The gage length, thickness and the diameter of the gage were measured. A total of 5 tensile tests were performed for each loading of GO to obtain average values. FESEM images were taken to examine the cross-section morphology of the fractured samples.

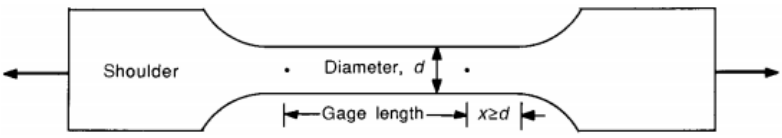

Figure 3.6: Specimen for Tensile Test

Figure 3.7: Tinius Olsen H10KS-0748

3.5.2 Water Absorption Test

Water absorption test was performed on nylon-6 and nylon-6/GO nanocomposites to study their water resistance properties. Specimens of dimensions 2mm x 2mm x 1mm were cut and dried at 80^{o}C in vacuum oven until the weight is constant. The samples were immersed in water at room temperature until no further increase in weight was observed. The samples were removed periodically and weighed on balance of 0.1mg precision. Prior to weighing, the specimens were wiped to remove excess water. The weight gained by the nanocomposites is determined by Equation 3.3:

$$M_t = \frac{W_w - W_d}{W_d} \; x \; 100\% \qquad (3.3)$$

where

W_d = weight of dry material prior to water immersion

W_w = weight of material after absorbing water

CHAPTER 4

RESULTS AND DISCUSSIONS

4.1 Characterization of GNF and Graphite Oxide

4.1.1 Fourier Transform Infrared Spectroscopy (FTIR)

FTIR was carried out to identify the functional groups in GNF and graphite oxide. Figure 4.1 shows the IR spectrum of GNF and graphite oxide scanned with wavelength ranged from 4000cm^{-1} to 400cm^{-1} with 4 scans at resolution of 4cm^{-1}. Table 4.1 summarizes the absorption frequency regions for the relevant functional groups in GNF and graphite oxide.

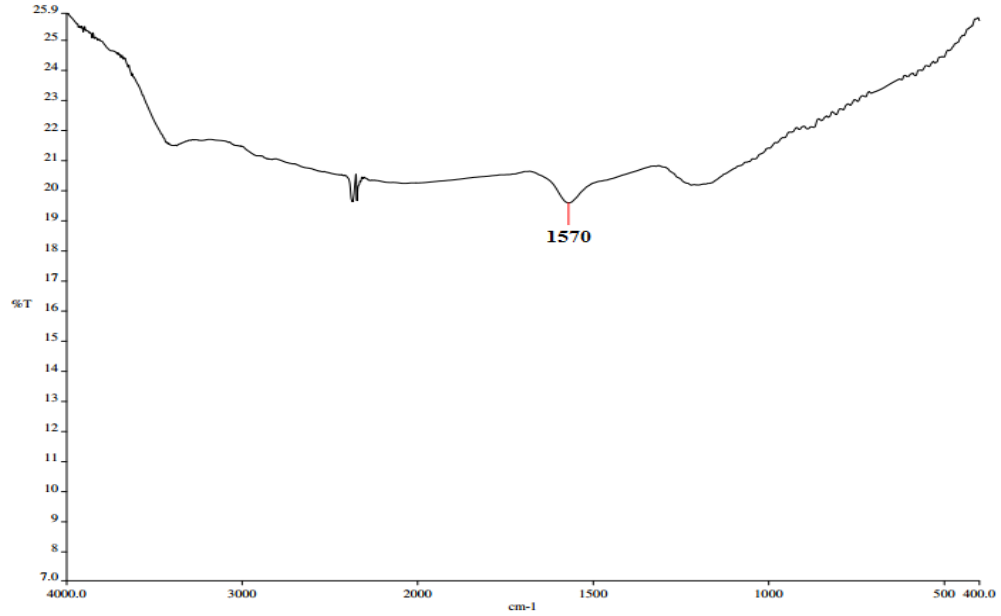

(a)

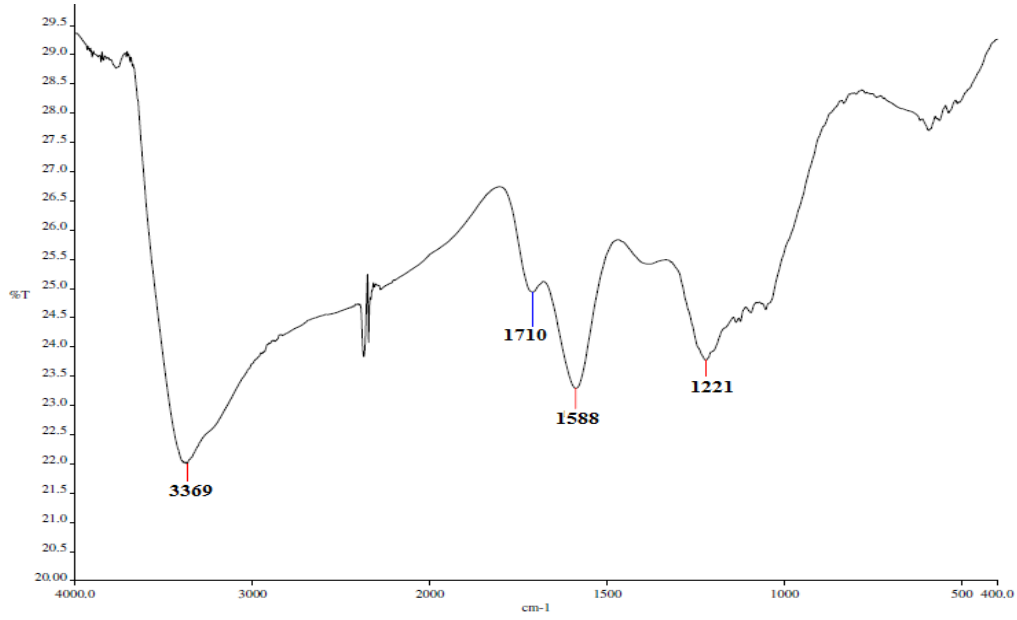

(b)

Figure 4.1: FTIR Spectra of (a) GNF and (b) Graphite Oxide

Table 4.1: Functional Groups and Absorption Frequency Regions

Absorption Frequency (cm^{-1})	Absorption Frequency (cm^{-1})		Functional Groups
	GNF	Graphite Oxide	
3200-3550		3369	Alcohol/Phenol OH Stretching
1710-1780		1710	Carboxylic C=O Stretching
1680-1750			Carbonyl C=O Stretching
1500-1700	1570	1588	Aromatic C=C Bending
1040-1240		1221	C-O-C Stretching
1000-1260			Alcohol C-O Stretch
1320-1210			Carboxylic C-O Stretch

The peak at $1570cm^{-1}$ indicates the presence of C=C bonds for GNF. For graphite oxide, peak at $1221cm^{-1}$ represents the vibration of C-O-C epoxide functional groups or C-O stretching of alcohol or carboxylic acid. Peak at $1588cm^{-1}$ gives indication of the unoxidised C=C bonds presence in graphite oxide. Another peak at $1710cm^{-1}$ evidences the stretching vibration of C=O. A very intense peak at $3369cm^{-1}$ signifies the stretching vibration of OH groups.

The IR spectrum of graphite oxide has demonstrated the successful oxidation of GNF using Hummer's Method through incorporation of oxygen-containing groups.

4.1.2 X-ray photoelectron spectroscopy (XPS)

XPS was employed to confirm the results obtained by the FTIR. Figure 4.2 displayed the XPS spectra of GNF and graphite oxide. Although GNF seems to have contained a certain amount of oxygen groups, the atomic concentration of oxygen (O) in graphite oxide is higher than that in GNF, stipulating the increase in oxygen functional groups in graphite oxide after oxidation. Four peaks were revealed in the detailed C1 s spectrum of GNF and graphite oxide in Figure 4.3. The peaks are assigned as follows: C-C to peak at 284eV, C-OH to 285eV, C=O to 287eV and COOH to 289eV which are in agreement with the study by Haubner et al. (2010). The spectrum demonstrated a slightly larger proportion C=O and C-O functionalities than COOH groups in graphite oxide and considerably higher amount of C-O in GNF. The intensity of the peaks of C=O and COOH in graphite oxide are much higher than that in GNF, indicating the presence of more oxygen groups at the edges of the graphitic layers after oxidation. This allows the formation of more interactions between these functional groups with other hydrophilic material as the edges have higher accessibility.

It is interesting to notice that the peak of Si-O present in GNF due to contamination became undetectable in graphite oxide from O1 s spectra in Figure 4.4. Si might be replaced in the process of graphite oxide synthesis and removed during the washing of graphite oxide paste.

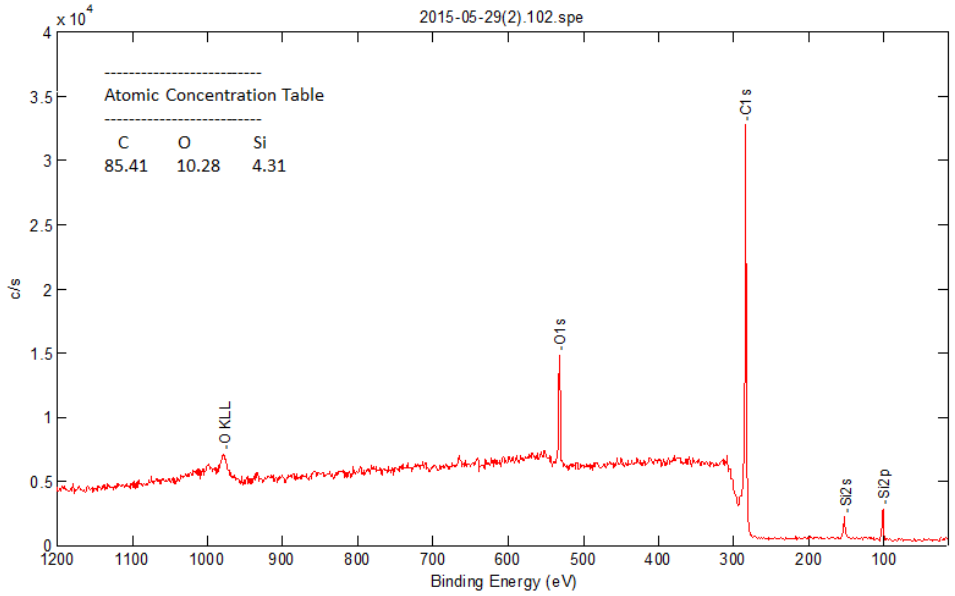

(a)

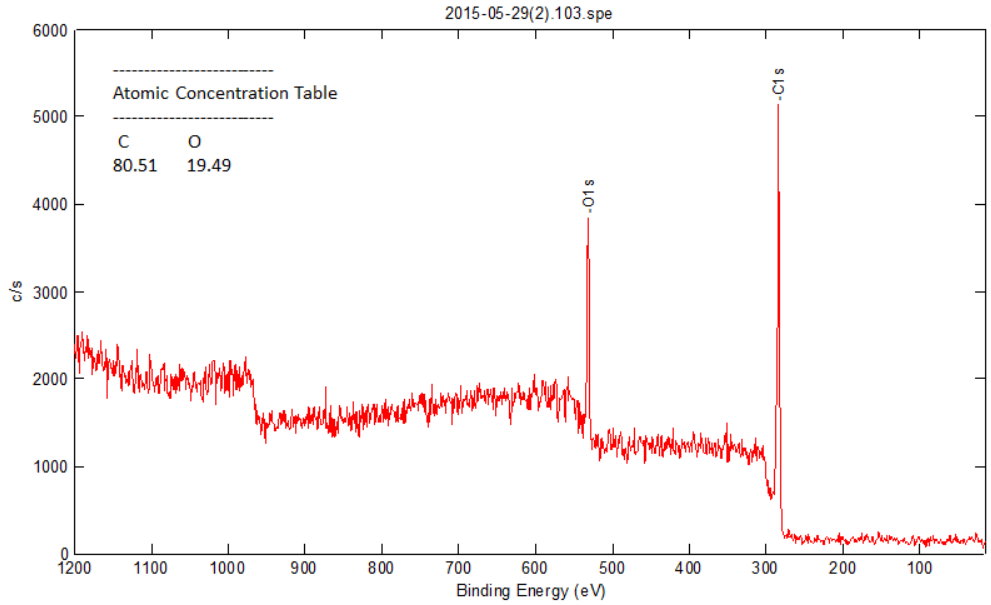

(b)

Figure 4.2: XPS Spectra of (a) GNF (b) Graphite Oxide

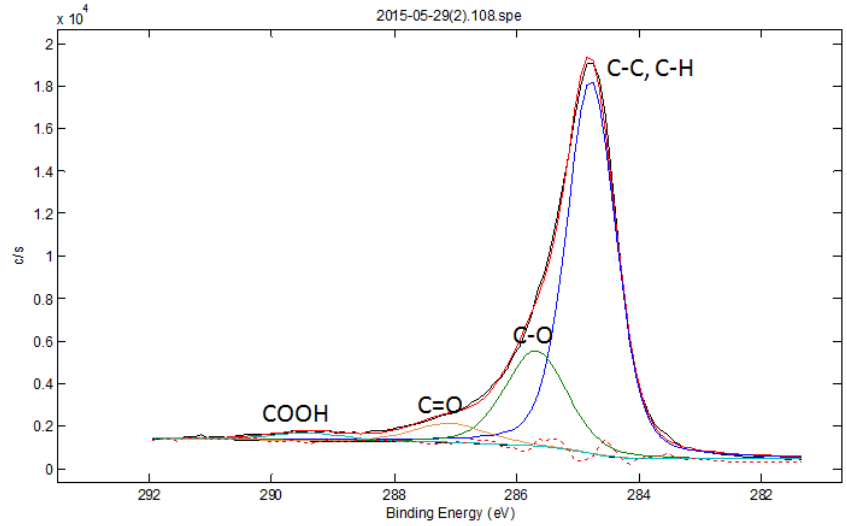

Atomic Concentration Table

C-C	C-O	C=O	COOH.
69.82	22.62	5.47	2.09

(a)

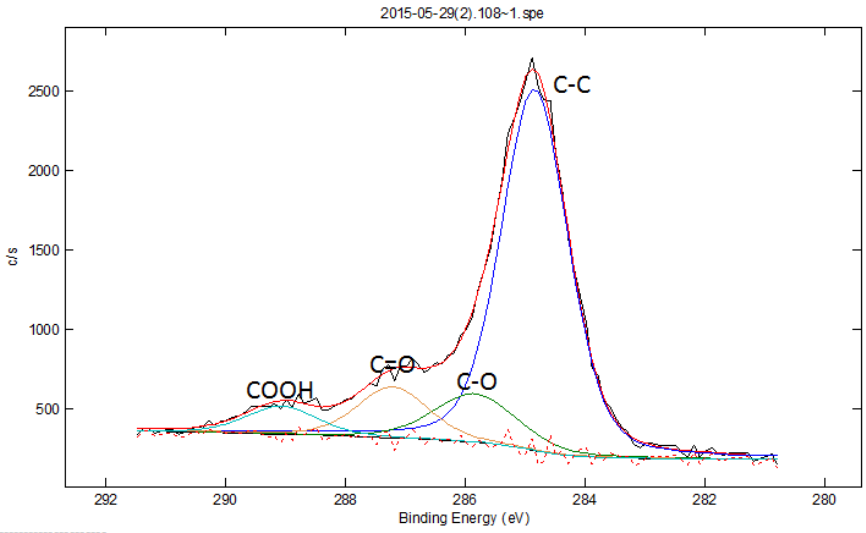

Atomic Concentration Table

C-C	C-O	C=O	COOH
71.61	11.83	10.66	5.91

(b)

Figure 4.3: C 1s Spectra of (a) GNF (b) Graphite Oxide

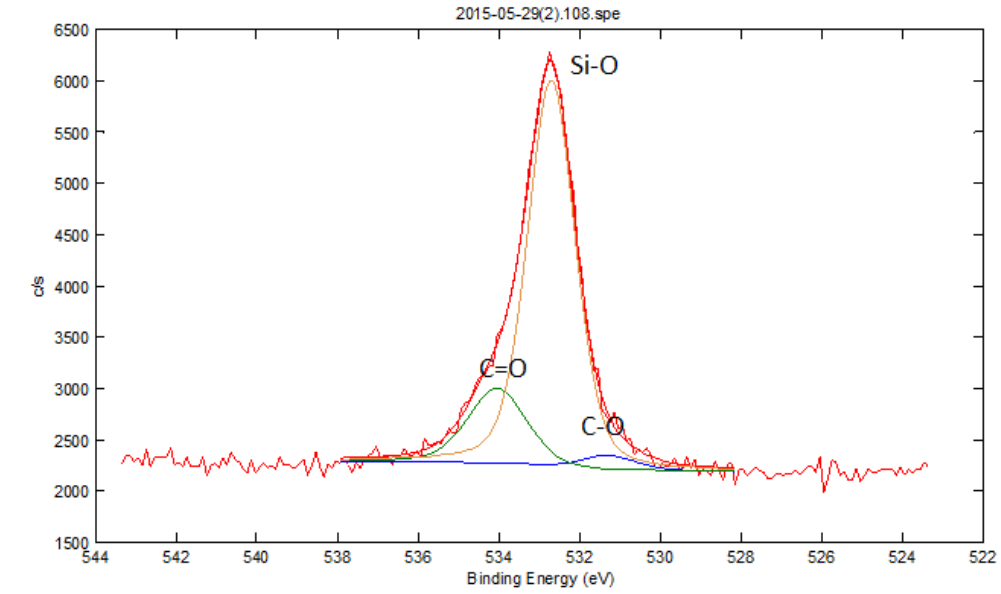

Atomic Concentration Table

C-O	C=O	Si-O
3.84	18.55	77.61

(a)

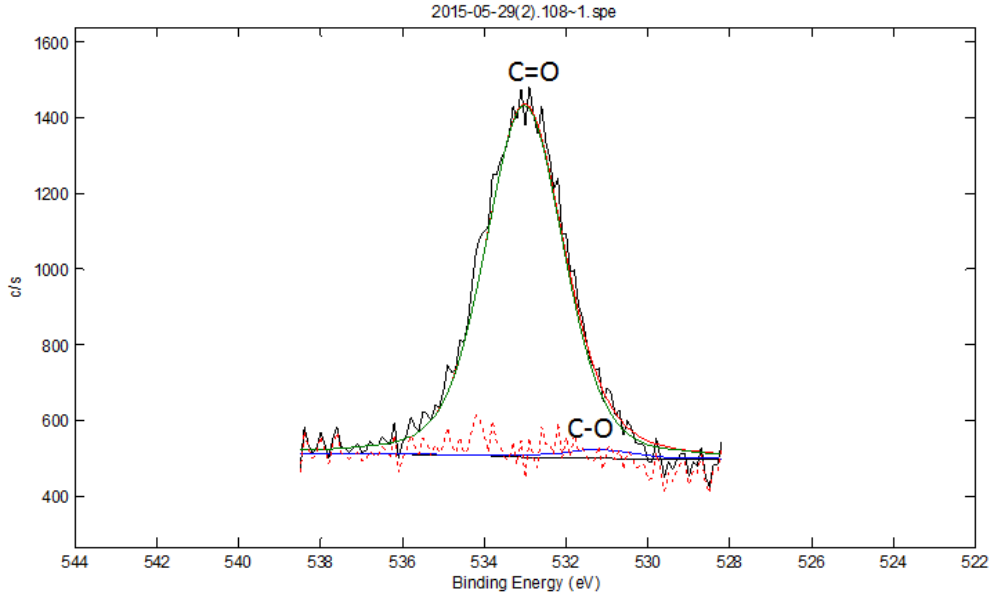

Atomic Concentration Table

C-O	C=O
2.29	97.71

(b)

Figure 4.4: O 1s Spectra of (a) GNF (b) Graphite Oxide

4.1.3 Raman Spectroscopy

The structural information on the carbon material was obtained by Raman Spectroscopy. The G band arising at 1587cm^{-1} in Raman spectrum of GNF in Figure 4.5 was attributed to the vibration of sp^2 carbon atoms. On the other hand, the D band appearing at 1349cm^{-1} reflected the defects at the edges of the graphitic layers. For the spectra of graphite oxide, a blueshift of 13cm^{-1} in the G band was found, stipulating successful oxidation of GNF (Li et al., 2014). The intensity ratios of the D and G band (I_D/I_G) for GNF and graphite oxide are 0.9998 and 1.0004 correspondingly. The increment in the value evidences the conversion of sp^2 state carbon atoms to sp^3 hybridized carbons (Tripathi et al., 2013).

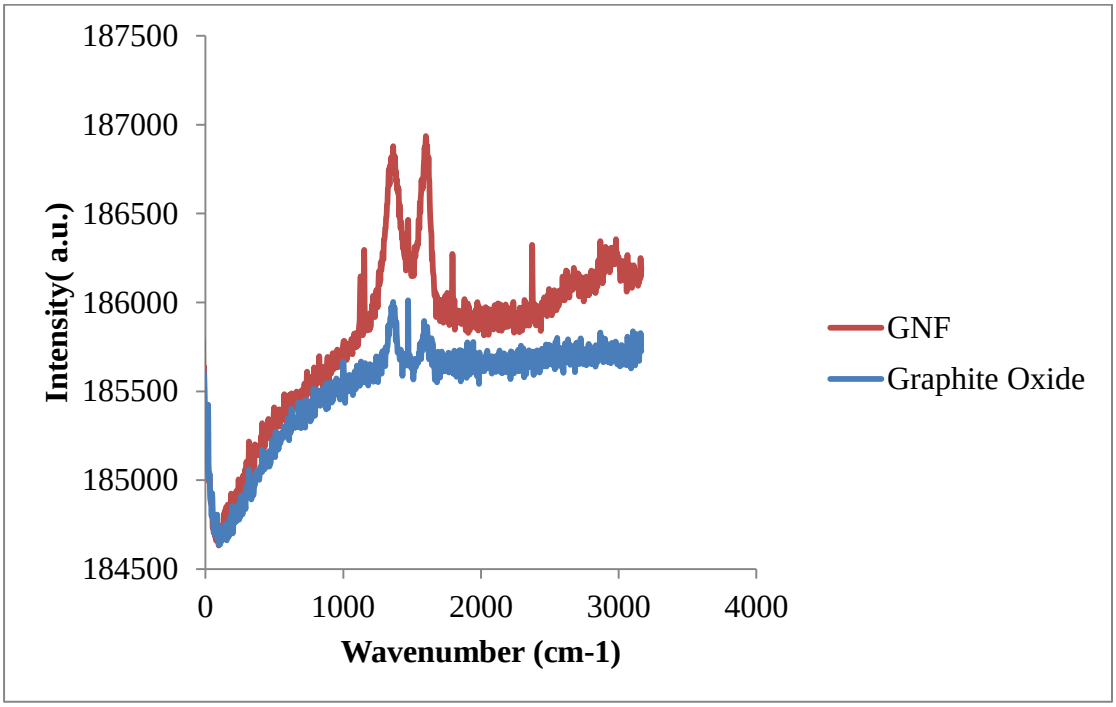

Figure 4.5: Raman Spectra of GNF and Graphite Oxide

4.1.4 X-Ray Diffraction (XRD)

The structure of GNF and graphite oxide was also analysed using XRD. The XRD Diffractogram for both GNF and graphite oxide is illustrated by Figure 4.6.

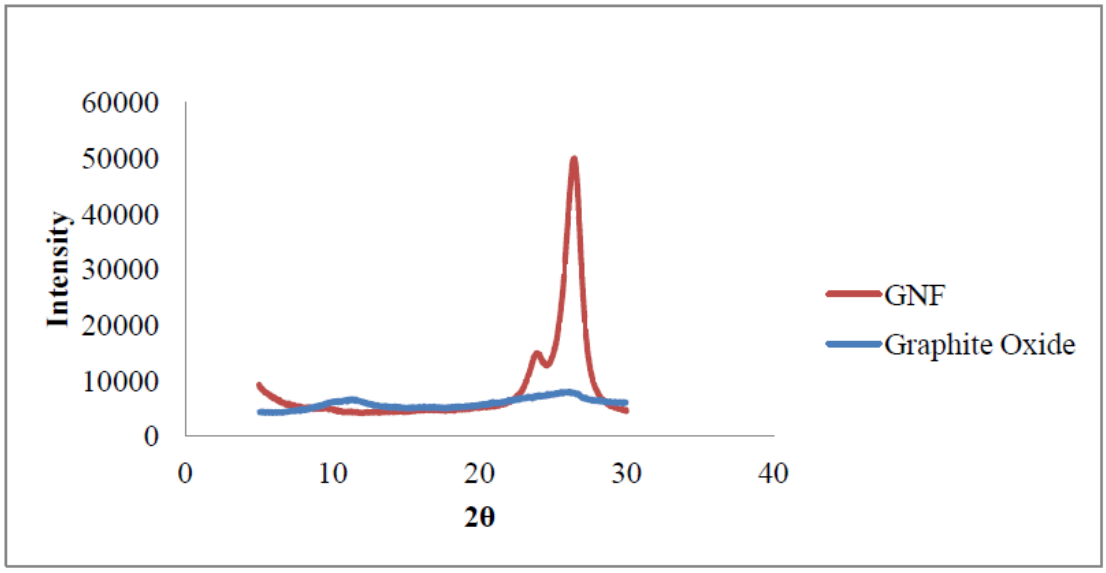

Figure 4.6: XRD Diffractogram of GNF and Graphite Oxide

The diffraction peak of GNF at 2θ= 26.3281^{o} corresponds to the spacing between the graphitic layers which is around 0.3382nm. On the other hand, graphite oxide gives a very low peak at the particular value, indicating the preservation of some unoxidized graphitic surfaces. Another peak arising at around 12^{o} corresponds to interlayer spacing of 0.7366nm. This proved the increment in interlayer spacing due to oxygen functionalities embedded in the layers as stated by Ciszewski and Mianowski (2013). In relation to this, Du, Qu and Zhang (2007) also reported a diffraction peak at 2θ= 12.02^{o} for graphite oxide.

Amorphous material produces broad and low intensity peak whereas crystalline material gives sharp and high intensity peaks. The degree of crystallinity is the ratio of intensity of crystalline peak to the total intensity of all peaks (Rigaku, 2015). Consequently, it can be deduced from Figure 4.6 that the crystallinity of GNF is much higher that than of graphite oxide.

4.1.5 Morphology Study

The morphology of GNF and graphite oxide was examined using FESEM. GNF possesses hair-like structure with smooth surfaces. As compared to GNF, graphite oxide exhibits much rougher surface as observed in Figure 4.7, similarly to the morphology reported by Bykkam et al. (2013). This is attributed by the oxygen-containing groups present on the surface of the graphitic layers.

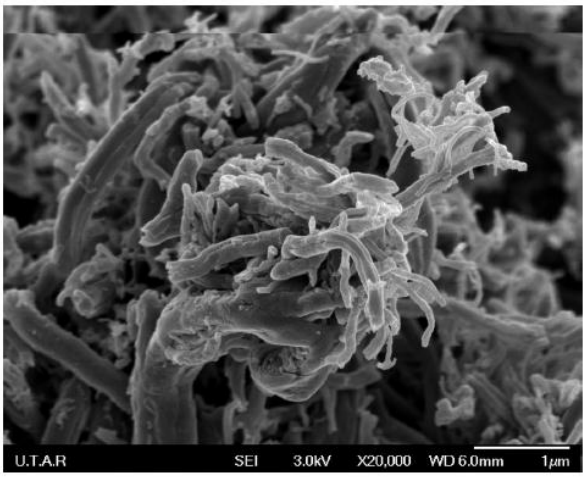

(a)

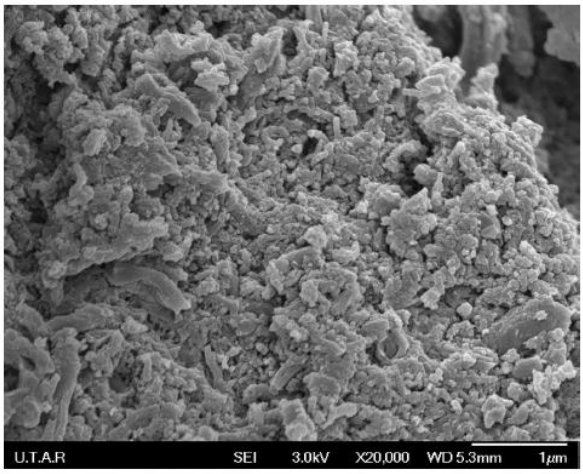

(b)

Figure 4.7: SEM Image of (a) GNF (b) Graphite Oxide

4.1.6 Thermal Decomposition Study

TGA was performed to determine the thermal stability of GNF and graphite oxide. The TGA traces are shown in Figure 4.8. Thermal degradation of material is identified by decrease in weight. Based on the curve for GNF, the thermal degradation of GNF was insignificant until the temperature reached approximately 700^{o}C. The total weight loss of GNF when heated from room temperature up to 800^{o}C was roughly 8%. This indicated the high thermal stability of GNF attributed to the strong C=C bonding between the sp^2 hybridized carbons. Comparatively, the reduction in the weight of graphite oxide was much more prominent than GNF.

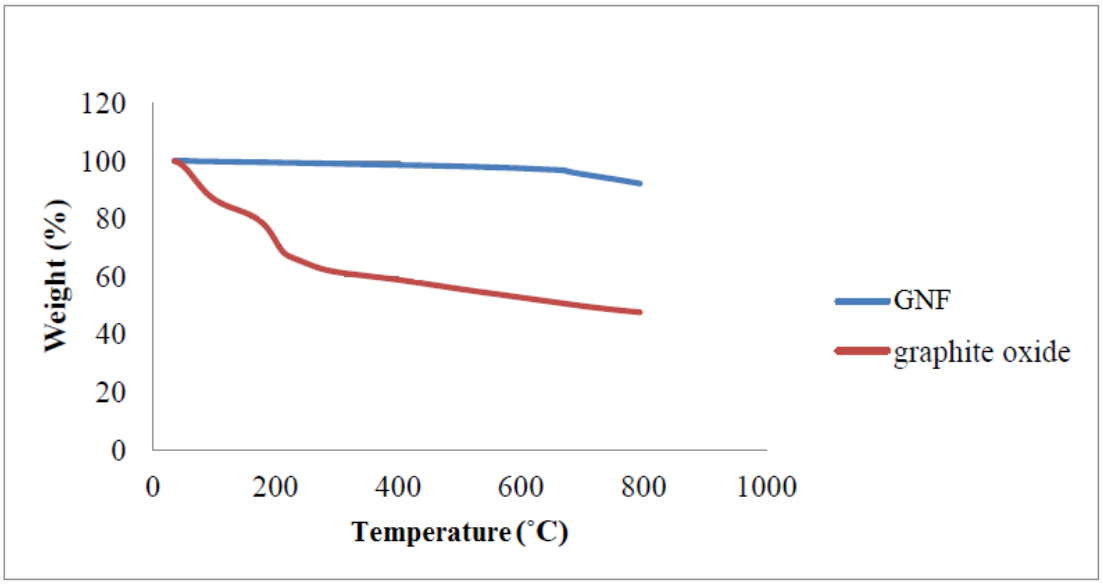

Figure 4.8: TGA Curves of GNF and Graphite Oxide

However the first weight loss for graphite oxide occurred at temperature below 150 ℃. The weight loss was due to the water molecules vaporizing out of the GO layers. At temperature above 150 ℃, oxygen functional groups such as carboxylic started to decompose, causing further weight loss. The thermal decomposition continued at temperature above 300 ℃ as more stable oxygen functionalities such as carbonyl and phenol began to break down (Haubner et al., 2010). Song, Wang and Chang (2014) stated that the carbon skeleton of graphite only decompose at temperature above 620 ℃. The total weight loss was approximately 52% for graphite oxide. In short, graphite oxide is not as thermally stable as GNF.

4.2 Processing Characteristics of Nylon-6/GO Nanocomposites

Figure 4.9 shows the torque during compounding of nylon-6 and nylon-6/GO nanocomposites as function of time. The process was carried out in Brabender rheometer at 235^{o}C for 7.5 minutes.

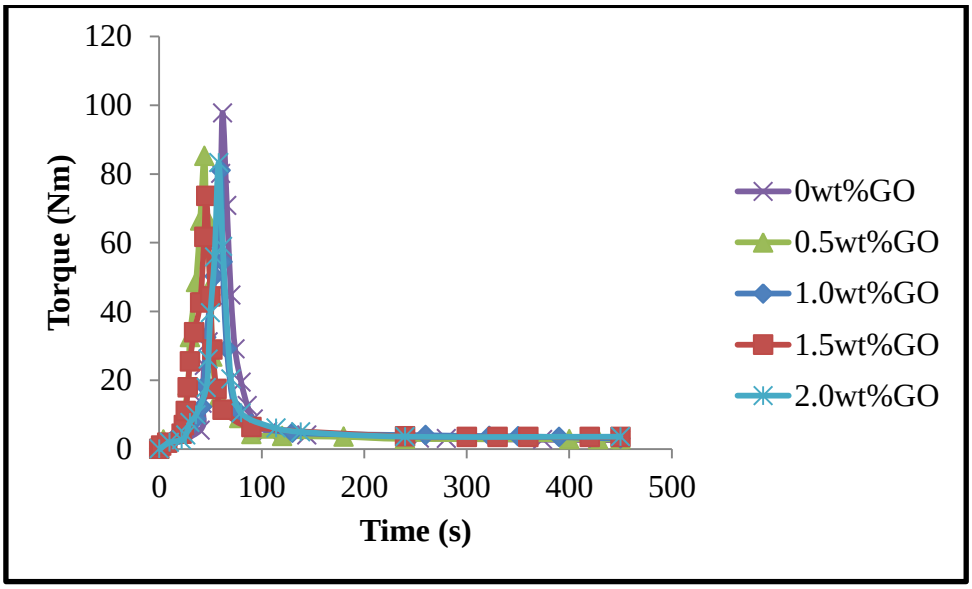

Figure 4.9: Torques for Neat Nylon-6 and Nylon-6 Nanocomposites during Compounding

The torques for all the samples rose steeply and reached the peak at the time of 40-70 seconds after the materials entered the mixing chamber. The solid pellets and GO resisted the rotation of the rotors by frictional force. As torque is the rotational force delivered by the mixer, larger force was required to turn the rotors at the specified speed. The torques declined sharply after reaching peaks, indicating melting of nylon-6 pellets. The torques reached almost stable values at around 100 seconds which indicates complete melting of nylon-6 pellets. The samples were allowed to mix for another 350 seconds to promote good dispersion of filler in the nylon-6 matrix. When the torque values were observed to be stable at time around 450 seconds the mixing was stopped. Stable value of torque is also known as stabilization torque which indicates the homogenous dispersion of filler in polymer melt (Demir et al., 2006).

At stabilization conditions, the effect of filler loading on the rheological behaviour of the composites can be studied by using torque as indicator of viscosity. The stabilization torques is very near to each other and hard to differentiate in Figure 4.9. In fact, the stabilization torque for the nylon-6/GO nanocomposites increased very slightly with increasing amount of GO. Figure 4.10 shows the stabilization torques of pure nylon-6 and nylon-6 nanocomposites.

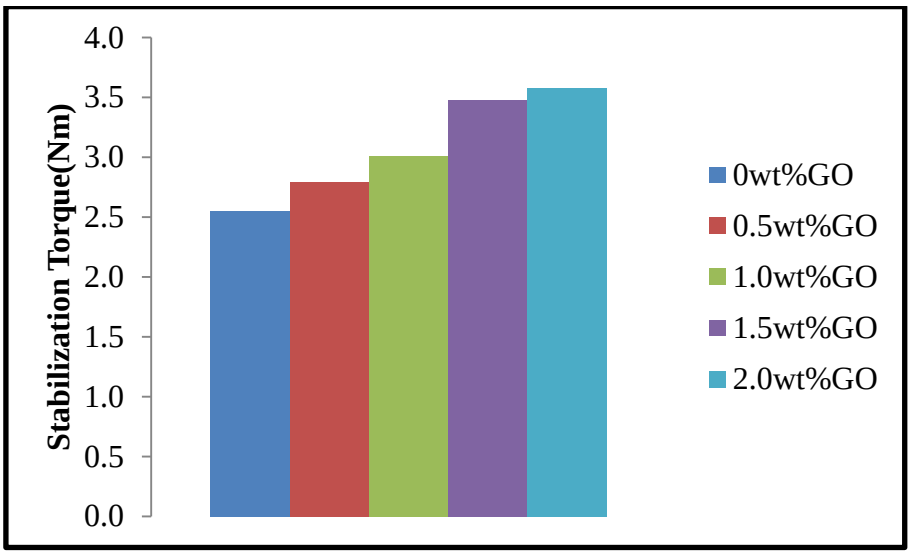

Figure 4.10: Stabilization Torques for Neat Nylon-6 and Nylon-6/GO Nanocomposites

GO contains oxygen functional groups that are able to form interactions with the polar functional groups of nylon-6. Increasing loading of GO enhanced the interactions between itself and the polymer matrix, thus reducing the mobility of the polymer chains. In other words, the viscosity enhanced. Therefore, higher shear or force was necessary to move the polymer melt hence higher stabilization torque resulted. Ghosh (2009) reported increasing stabilization torque with increasing percentage of carbon nanofibre in polypropylene. Although the stabilization torques was getting larger, the extent of increment was very low which may avoid difficulty in processing and product fabricating where nylon-6/GO nanocomposites are used.

4.3 Characterization of Nylon-6/GO Nanocomposites

4.3.1 Fourier Transform Infrared Spectroscopy (FTIR)

FTIR was carried out as a qualitative measurement on the chemical structure of neat nylon and nylon-6/GO nanocomposites. Based on the IR spectra of nylon in Figure 4.11, the peak observed at 3292cm^{-1} represents N-H stretching. Anti-symmetric CH_2 stretching appears at 2937cm^{-1} while symmetric CH_2 stretching is visible at 2861cm^{-1}. Peak at 1631cm^{-1} corresponds to C=O stretching. Absorption at 1538cm^{-1} is due to the presence of N-H bending in plane. There are also peaks at 1462cm^{-1}, 1417cm^{-1} and 1202cm^{-1} which are assigned to CH_2 symmetric bending, O-H bending and C-N stretching of amine respectively (Bhattacharya and Mandot, 2013). The assignment of the functional groups is summarized in Table 4.2.

Table 4.2: Assignment of Functional Groups to Peaks in IR Spectra

Frequency (cm^{-1})	Functional Group
3292	N-H stretching
2937	Anti-symmetric CH_2 stretching
2861	Symmetric CH_2 stretching
1631	C=O stretching
1548	N-H bending
1462	CH_2 symmetric bending
1417	O-H Bending
1202	C-N stretching

Compared to the spectra of the neat nylon in nylon-6/GO nanocomposites Figure 4.11, N-H stretching at 3292cm^{-1} shifted to higher wavenumber at 3299cm^{-1}, 3296cm^{-1}, 3307cm^{-1} and 3298cm^{-1}. Peak at 1631cm^{-1} due to C=O stretching shifted to 1636cm^{-1}, 1640cm^{-1} and 1643cm^{-1} while peak at 1548cm^{-1} corresponding to N-H bending shifted to 1551cm^{-1} and 1552cm^{-1}. This was due to the polar functional groups N-H and C=O forming hydrogen bonding with GO which possess oxygen containing groups such as –OH, C-O-C and C=O. Figure 4.12 illustrates the formation

of hydrogen bonding between GO and nylon-6. Study by Jin et al. (2013) revealed the shifting of characteristic peaks of N-H to higher frequency due to the formation of hydrogen bonding between N-H groups in nylon-11 and COOH groups of functionalized graphene. Peak at 1718cm^{-1} which is attributed by C=O stretching in GO became more visible in the nanocomposites. The other functional groups of GO including C-O-C Stretching at 1221cm^{-1}, OH Stretching at 3369cm^{-1} and C=C Bending at 1588cm^{-1} are not visible as individual peaks as they overlap with broad peaks given rise by nylon.

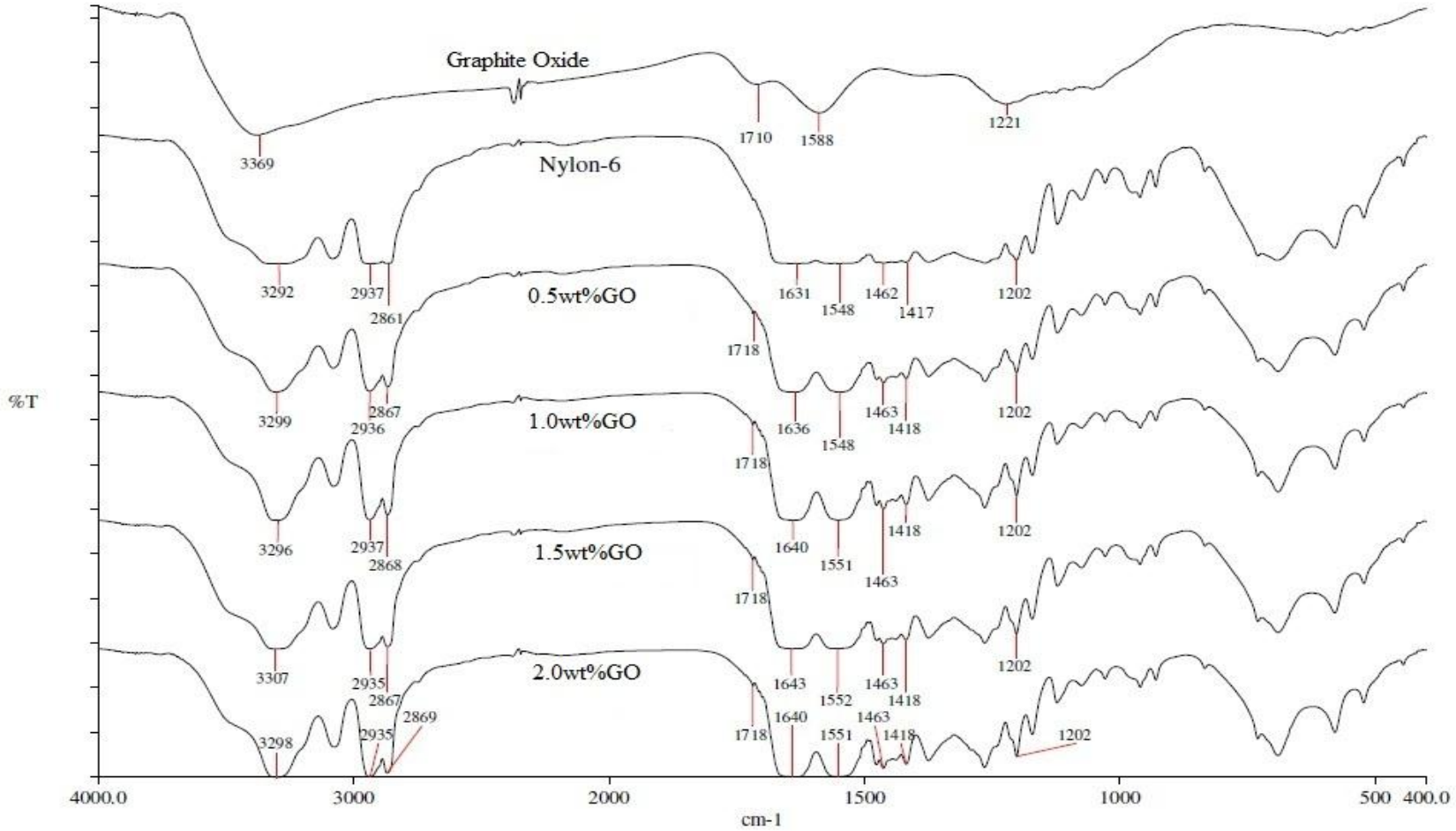

Figure 4.11: IR Spectra of Graphite Oxide, Nylon-6 and Nylon-6 Nanocomposites

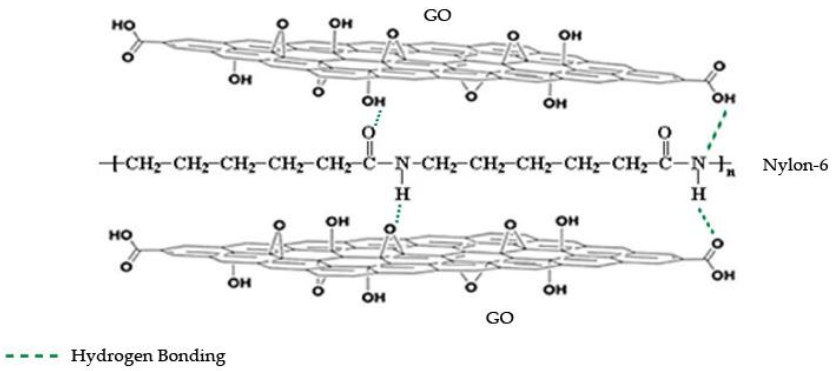

Figure 4.12: Hydrogen Bonding between GO and Nylon-6

4.3.2 Thermal Properties of the Nanocomposites

Thermal analysis was carried out with DSC to elucidate the melting behavior of the neat nylon and nylon nanocomposites by heating from room temperature to 300^{o}C at 10^{o}C/min. DSC heating scans in Figure 4.13 shows that there was no significant effect of GO loading on the peak melting temperature (T_m) of the nanocomposites as compared to the neat nylon. The increment in the crystallization temperature (T_c) was more prominent. This might be caused by the good thermal conductivity of GO compared to nylon-6 polymer matrix. Heat could be extracted out more easily and thus nucleation could occur at higher temperature when GO loading increased. A study by Mert (2007) presented higher temperature to reach the maximum crystallization rate for polyamide-66 nanocomposites than for pure polyamide-66 due to the presence of montmorillonite layers which act as active sites for heterogeneous nucleation through which crystallization proceeds. Allafi and Pascal (2012) suggested that the increase in crystallization temperature would be beneficial to the industry due to lesser solidification time after processing. However the degree of crystallinity (X^m_c) decreased as the presence of GO restricted the formation of large crystalline structures in nylon-6 (Allafi and Pascal, 2012).

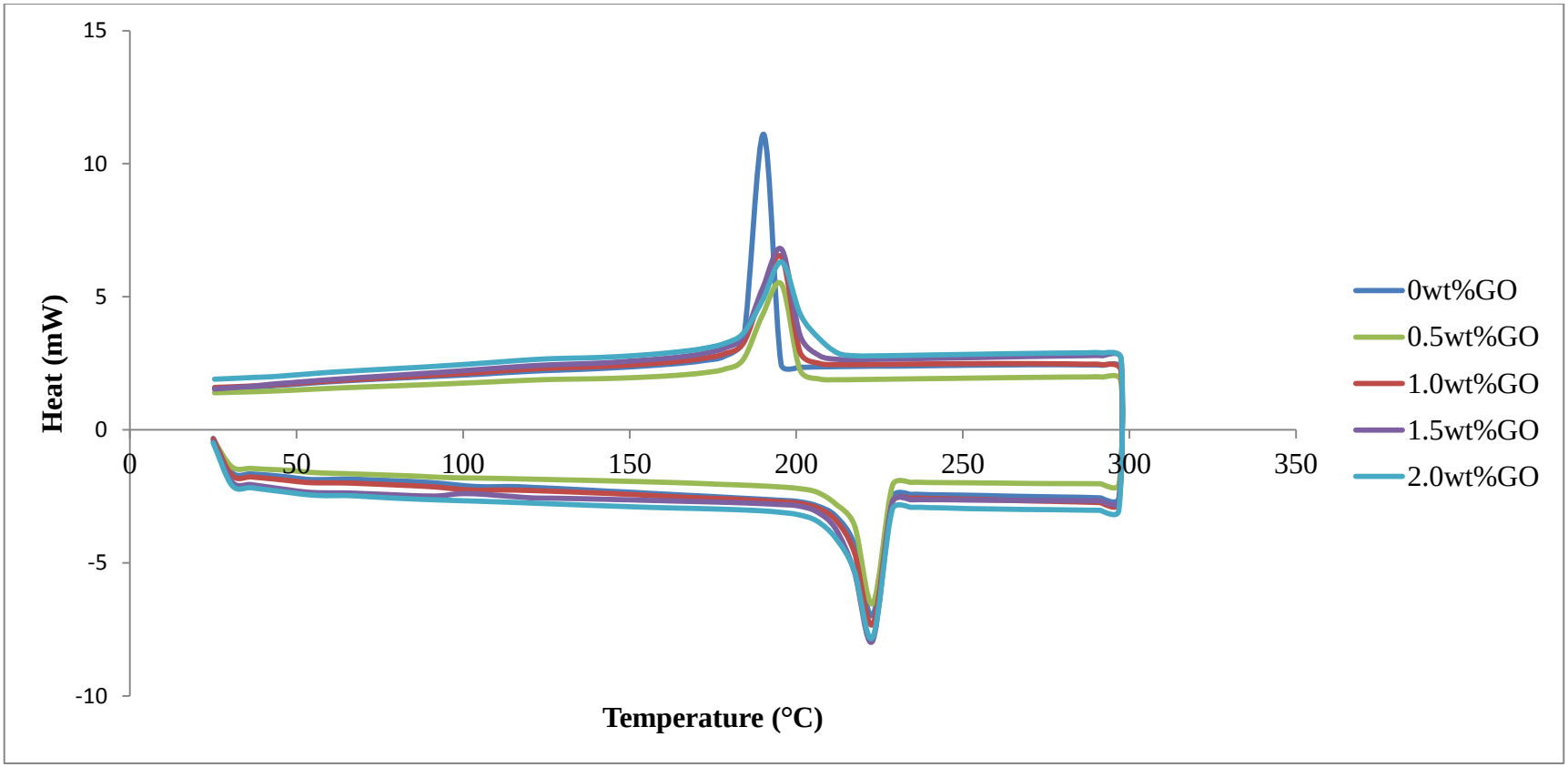

Figure 4.13: DSC Curves for Nylon-6/GO Nanocomposites

Table 4.3: DSC Results of Nylon-6/GO Nanocomposites

GO Loadings (wt%)	T_m(^oC)	ΔH_m (J/g)	X^m_c	T_c (^oC)
0	224.54	88.32	36.8	190.91
0.5	223.95	78.39	32.82	193.96
1.0	223.92	73.30	30.85	194.01
1.5	223.72	71.48	30.24	194.35
2.0	224.18	73.72	31.34	195.15

4.3.3 Melt Flow Index (MFI)

The viscosities of nylon-6 and nylon-6/GO nanocomposites were measured by their respective MFI values. Table 4.4 records the MFI values of neat nylon-6 and its nanocomposites.

Table 4.4: MFI Values of Neat Nylon-6 and Its Nanocomposites

GO Loadings (wt%)	MFI(g/10min)
0	33.45
0.5	32.93
1.0	32.88
1.5	32.68
2.0	32.56

All nanocomposites gave slightly lower MFI values than the neat nylon-6. The increment in viscosity of the nanocomposites was contributed by the interactions formed between polymer chains and GO. The presence of these interactions makes the segmental motion of the polymer chains more difficult, causing greater flow activation energy (Barus et al., 2010). Since the polymer chains moves slower, the viscosity of the nanocomposites are slightly higher. By looking at bigger picture, the MFI values did not show significant difference among the 5 samples where the

difference between any 2 values does not exceed 1g/10min. This indicated that the incorporation of GO did not affect the process ability of the nylon-6.

4.3.4 Thermal Decomposition Study

The thermal stability of nylon-6 and the nanocomposites was investigated by TGA under nitrogen flow. All the samples underwent single step decomposition and this shows that GO did not alter the decomposition pathway of nylon-6. However, the TGA traces in Figure 4.14 stipulated that the onset of the thermal decomposition has shifted to higher temperature after GO was infused. Specifically, the onset decomposition temperature at weight loss of 5% for nylon-6/2.0wt% GO was 25^{o}C higher than the neat nylon-6. The weight loss of all nanocomposites denoted a shift towards higher temperatures. Other than that, the percentage of total weight loss at 750^{o}C was lower when the GO content in the nylon-6 is greater as tabulated in Table 4.5. The well dispersed GO can form a char layer on the nylon-6 nanocomposites. The formation of char acts as the barrier hindering the out-diffusion of the decomposition products which are volatile (Morimune, Nishino and Goto, 2012; Liu et al., 2003). Therefore, GO enhanced the thermal stability of nylon-6 by reducing the weight loss due to permeability of decomposed product.

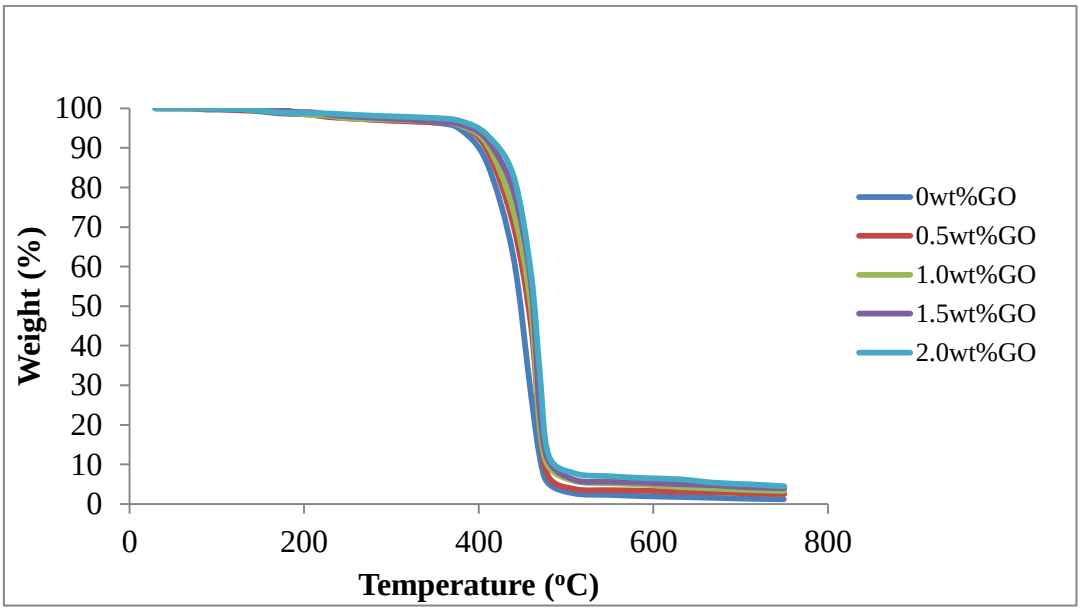

Figure 4.14: TGA Results of Nylon-6 and Nylon-6 Nanocomposites

Table 4.5: Temperature at 5wt% Weight Loss and Total Weight Loss at 750^{o}C

GO Loadings (wt%)	Temperature (^{o}C) at 5wt% Weight Loss	Total Weight Loss at 750^{o}C (g)
0	385	98.81
0.5	390	97.48
1.0	400	96.72
1.5	405	96.03
2.0	410	95.52

4.4 Performance Tests of Nylon-6/GO Nanocomposites

4.4.1 Tensile Test

The mechanical properties of the nylon-6/GO nanocomposites were studied by tensile test. Figure 4.15- 4.17 illustrates the trend of the elastic modulus, ultimate tensile strength and elongation at break of nylon-6 and its nanocomposites. The modulus, strength and elongation at break are summarized in Table 4.6.

The Young's Modulus is ratio of the stress to the strain which measures the stiffness of a material. The tensile strength is the maximum stress that a material can bear before breaking. The modulus and tensile strength showed an increasing trend with increasing percentage of GO in nylon-6. This was due to the reinforcement effect of GO possessing very high stiffness and strength. Strong interfacial interactions between GO and the nylon-6 matrix also enabled the external load to be efficiently transferred through the interactions. Chow and Ishak (2007) stated that the interaction of polymer chains with filler surfaces constrict the movement of the chains and may improve the modulus.

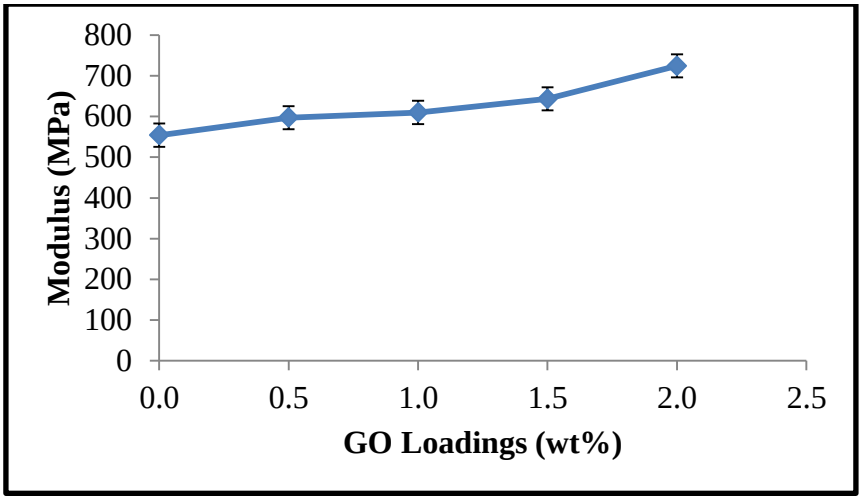

Figure 4.15: Young's Modulus of Nylon-6/GO Nanocomposites

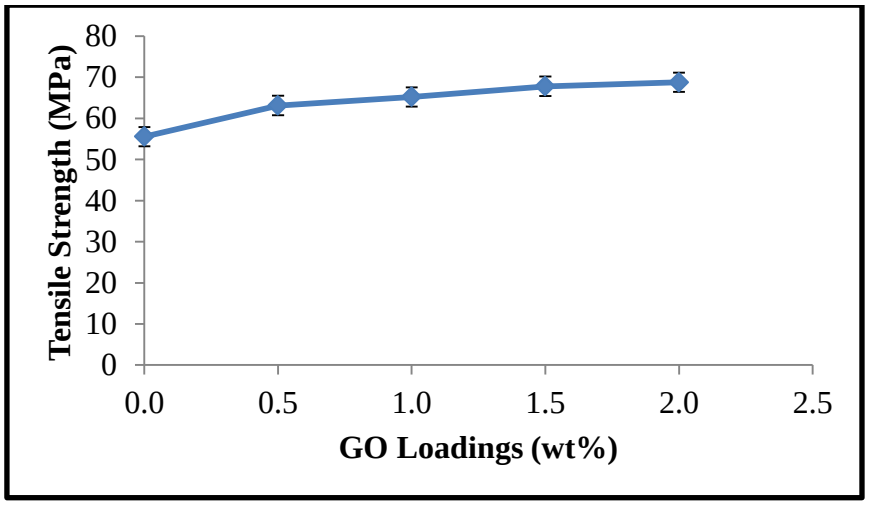

Figure 4.16: Tensile Strength of Nylon-6/GO Nanocomposites

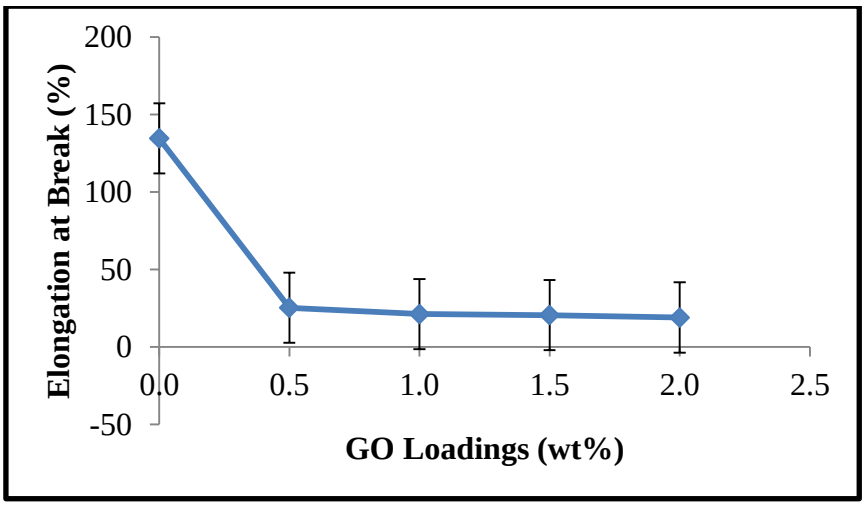

Figure 4.17: Elongation at Break of Nylon-6/GO Nanocomposites

Table 4.6: Mechanical Properties of Nylon-6 and Nylon-6/GO Nanocomposites

GO Loadings (wt%)	Young's Modulus (MPa)	Tensile Strength (MPa)	Elongation at Break (%)
0	554.43	55.56	134.61
0.5	597.14	63.13	25.28
1.0	610.00	65.23	21.26
1.5	643.33	67.80	20.57
2.0	724.40	68.78	19.02

The cross section morphology of the fractured nanocomposites was studied by SEM at magnification of X500 as shown in Figure 4.18. When the morphology of nylon-6/GO nanocomposites is put into comparison with the neat nylon, the surface is much rougher. This is due to the ability of GO in deflecting crack in the polymer matrix, causing the crack to follow a tortuous path which tend to stop the propagation of the crack.

Good dispersion of filler is also necessary for improvement in mechanical properties (Liu et al., 2003). From SEM images of the fracture surface of nylon-6 nanocomposites, GO was dispersed well in nylon-6 matrix without agglomeration. On the other hand, the elongations at break decreased with increasing amount of GO incorporated, indicating increasing brittleness of the nanocomposites.

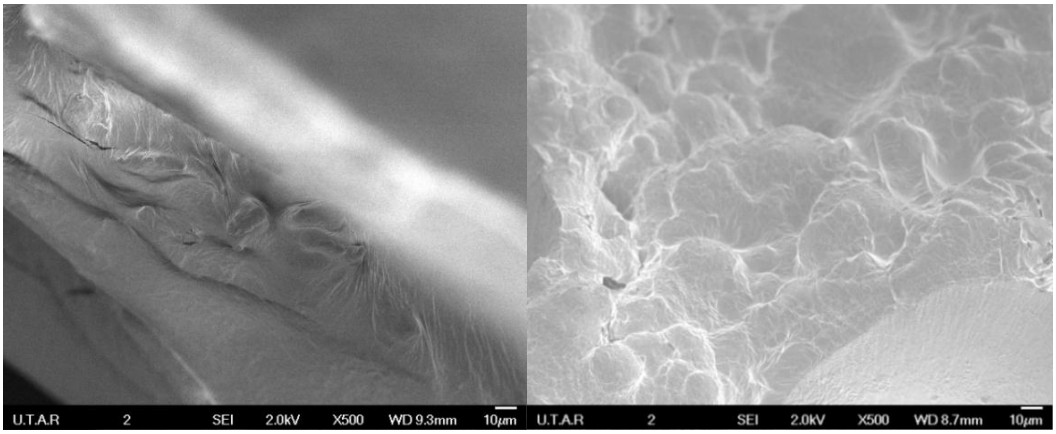

(a) (b)

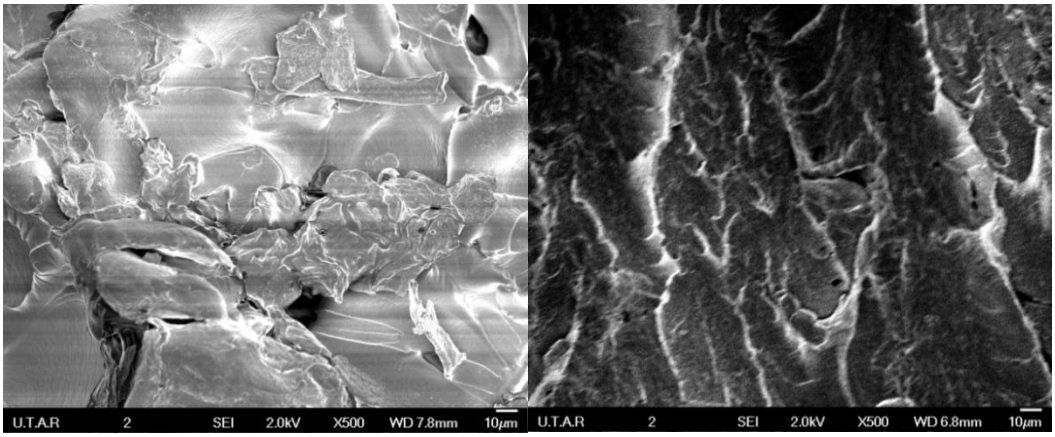

(c) (d)

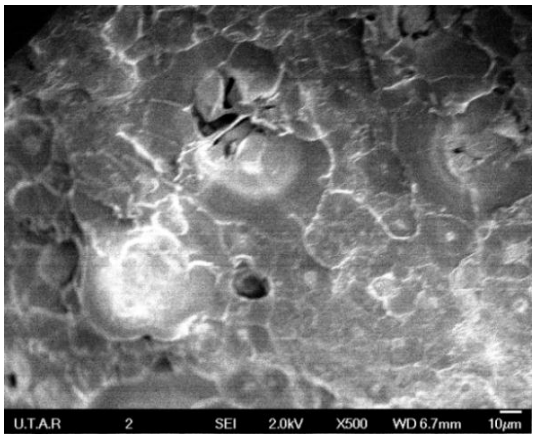

(e)

Figure 4.18: SEM Images of Nylon-6 Nanocomposites with (a) 0wt% GO (b) 0.5wt% GO (c) 1.0wt% GO (d) 1.5wt% GO (e) 2.0wt% GO at Magnification of 500X

4.4.2 Water Absorption Test

The water absorption test was performed under room temperature until the weight of the samples achieved constant values. Figure 4.19 and Table 4.7 present the results of water absorption test.

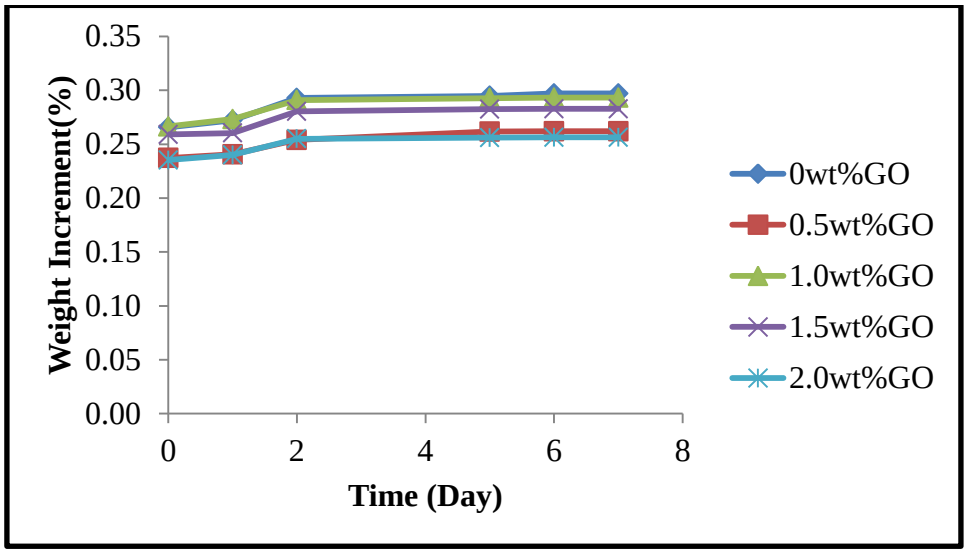

Figure 4.19: Water Absorption of Nylon-6 and Nylon-6/GO Nanocomposites

Table 4.7: Percentage Increment in Weight of Nylon-6 and Nylon-6/GO Nanocomposites

Day	Average Weight of 3 Nylon-6 Nanocomposite Replicates(g)				
	0wt%GO	0.5wt%GO	1.0wt%GO	1.5wt%GO	2.0wt%GO
0	0.2657	0.2373	0.2665	0.2591	0.2353
1	0.2722	0.2407	0.2732	0.2604	0.2400
2	0.2928	0.2539	0.2909	0.2805	0.2550
5	0.2948	0.2617	0.2929	0.2825	0.2561
6	0.2971	0.2620	0.2931	0.2828	0.2564
7	0.2971	0.2621	0.2931	0.2829	0.2564
Fractional Increment in Weight	0.1183	0.1045	0.1001	0.0917	0.0895

According to Figure 4.19 and Table 4.7, there was no further increment in the weight of nylon-6 nanocomposites from day 6 onwards. This indicated that the nanocomposites had absorbed the maximum amount of water within a week. The amount of water absorbed was calculated by deriving the percentage increase in the weight of the nanocomposites. Comparing the water absorption capability of all samples, increasing percentage of GO has contributed to better water resistance of nylon-6. The filler layers in the polymer increase the diffusion path length of water through the polymer. This attributes to the better barrier properties of nanocomposites (Abacha, Kubouchi and Sakai, 2009). This finding proves that the GO filler had dispersed well in the nylon-6 and there was no agglomeration.

CHAPTER 5

CONCLUSION AND RECOMMENDATIONS

5.1 Conclusion

Nylon-6/GO nanocomposites were successfully fabricated through melt mixing method. Graphite oxide was produced from GNF via conventional Hummers method. FTIR, XPS, Raman Spectroscopy, SEM, XRD and TGA analysis were carried out to proof the successful oxidation of GNF into graphite oxide. Characterization of nylon-6/GO nanocomposites by FTIR indicated the presence of GO in nylon-6. Peaks at 3292cm^{-1} due to N-H stretching, at 1631cm^{-1} due to C=O stretching, at 1548cm^{-1} corresponding to N-H bending shifted to higher wavenumber. DSC results showed lower crystallinity of the nanocomposites than the neat nylon-6. However, the melting temperature differed only very little. On the other hand, the crystallization temperatures were increasing with higher GO content. This results indicates that incorporation of GO allows the nanocomposites to be processed at the similar temperature as neat nylon-6 and in addition to that less cooling energy is needed for crystallization. The torque curve during processing also shows very small increment in resistance to rotation of the screw when GO was used. MFI values of the nanocomposites of different GO loadings were similar. These results illustrate similar process ability of the neat nylon-6 and nylon-6 nanocomposites. The TGA traces confirmed the better thermal stability of the nanocomposites by increment of 20^{o}C of onset decomposition temperature at 2wt% GO. Tensile test stipulated an increasing Young's Modulus and tensile strength of the nylon-6 with higher GO content. Both of the modulus and strength attained the highest values at 2wt% of GO at 724.4MPa and 68.78MPa, with percentage enhancement of 30.7% and 23.8% respectively.

Meanwhile, the elongation at break dropped from 134.61% to 19.02% with diminishment of 85.87 %. Rougher surfaces of the nanocomposites were observed through SEM, denoting the ability of GO in deflecting cracks. Nylon-6/GO nanocomposites indicated lower water absorbing characteristics than nylon-6 which is more desirable. Neat nylon-6 indicated an increment in weight of 11.83% after absorbing water while that for nylon-6 with 2wt% GO was 8.95%.

5.2 Recommendation

This study has demonstrated the enhanced mechanical and thermal properties of nylon-6/GO nanocomposites. The potential of GO as a promising filler in nylon-6 has been proven. Some steps can be done in order to optimise the process and properties of the nanocomposites.

- Further increase the percentage weight of GO in nylon-6 to investigate the maximum loadings of GO before onset of reduction in mechanical properties. Too high in GO content may cause the filler to agglomerate and the nanocomposite to be too brittle and breaks easily. This would be helpful in determining the filler content to be added in the manufacturing industry.

- Determine the dispersion pattern of GO in polymer matrix. The dispersion pattern may affect the properties of the nanocomposites produced. This can be done by Transmission Electron Microscopy (TEM).

- Prior exfoliation may further increase the surface-to-volume ratio of GO in the polymer matrix and bring greater improvement in the properties.

- Investigate the performance of nylon-6 nanocomposites incorporated with surface-treated GO.

REFERENCES

Abacha, N., Kubouchi, M. and Sakai, T. (2009). Diffusion behavior of water in polyamide 6 organoclay nanocomposites. *expresspolymlett*, 3(4), pp.245-255.

Allafi, A. and Pascall, M. (2013). The effect of different percent loadings of nanoparticles on the barrier and thermal properties of nylon 6 films. *Innovative Food Science & Emerging Technologies*, 20, pp.276-280.

Anandhan, S. and Bandyopadhyay, S. (2011). Polymer Nanocomposites: From Synthesis to Applications. *Nanocomposites and Polymers with Analytical Methods*.

Barus, S., Zanetti, M., Bracco, P., Musso, S., Chiodoni, A. and Tagliaferro, A. (2010). Influence of MWCNT morphology on dispersion and thermal properties of polyethylene nanocomposites. *Polymer Degradation and Stability*, 95(5), pp.756-762.

Bhattacharya, S. and Mandot, A. (2015). Polyamide/Clay Nanocomposites Film, Synthesis and Mechanical Testing. *International Journal of Pure and Applied Sciences and Technology*, 17(2), pp.36-44.

Brodie, B. (1859). On the Atomic Weight of Graphite. *Philosophical Transactions of the Royal Society of London*, 149, pp.249-259.

Bykkam, S., Rao K., V., Chakra CH., S. and Thunugunta, T. Synthesis and Characterization of Graphene Oxide and Its Antimicrobial Activity against Klebseilla and Staphylococus. *International Journal of Advanced Biotechnology and Research*. 2013; 4(1): 142-146.

Chen, D., Zhu, H. and Liu, T. (2010). In Situ Thermal Preparation of Polyimide Nanocomposite Films Containing Functionalized Graphene Sheets. *ACS Appl. Mater. Interfaces*, 2(12), pp.3702-3708.

Cheran, L., Cheran, A. and Thompson, M. (2014). CHAPTER 1. Biomimicry and Materials in Medicine. *RSC Detection Science*, pp.1-25.

Chow, W. (2007). Water absorption of epoxy/glass fiber/organo-montmorillonite nanocomposites.*expresspolymlett*, 1(2), pp.104-108.

Chow, W. and Mohd Ishak, Z. (2007). Mechanical, morphological and rheological properties of polyamide 6/organo-montmorillonite nanocomposites. *expresspolymlett*, 1(2), pp.77-83.

Ciszewski, M. and Mianowski, A. (2013). *Survey of graphite oxidation methods using oxidizing mixtures in inorganic acids - Chemik International*. [online] Chemik International. Available at: http://www.chemikinternational.com/year-2013/year-2013-issue-4/survey-of-graphite-oxidation-methods-using-oxidizing-mixtures-in-inorganic-acids/ [Accessed 11 Mar. 2015].

Corcione, C. and Frigione, M. (2012). Characterization of Nanocomposites by Thermal Analysis.*Materials*, 5(12), pp.2960-2980.

Cote, L., Kim, F. and Huang, J. (2009). Langmuir−Blodgett Assembly of Graphite Oxide Single Layers. *J. Am. Chem. Soc.*, 131(3), pp.1043-1049.

Cunha, E., Paiva, M., Hilliou, L. and Covas, J. (2015). Tracking the progression of dispersion of graphite nanoplates in a polypropylene matrix by melt mixing. *Polym. Compos.*, p.n/a-n/a.

Demir, H., Atikler, U., Balköse, D. and Tıhmınlıoğlu, F. (2006). The effect of fiber surface treatments on the tensile and water sorption properties of polypropylene–luffa fiber composites.*Composites Part A: Applied Science and Manufacturing*, 37(3), pp.447-456.

Dhand, V., Rhee, K., Ju Kim, H. and Ho Jung, D. (2013). A Comprehensive Review of Graphene Nanocomposites: Research Status and Trends. *Journal of Nanomaterials*, 2013, pp.1-14.

Dreyer, D., Park, S., Bielawski, C. and Ruoff, R. (2010). The chemistry of graphene oxide. *Chem. Soc. Rev.*, 39(1), pp.228-240.

Du, L., Qu, B. and Zhang, M. (2007). Thermal properties and combustion characterization of nylon 6/MgAl-LDH nanocomposites via organic modification and melt intercalation. *Polymer Degradation and Stability*, 92(3), pp.497-502.

Du, Q., Zheng, M., Zhang, L., Wang, Y., Chen, J., Xue, L., Dai, W., Ji, G. and Cao, J. (2010). Preparation of functionalized graphene sheets by a low-temperature thermal exfoliation approach and their electrochemical supercapacitive behaviors. *Electrochimica Acta*, 55(12), pp.3897-3903.

Erickson, K., Erni, R., Lee, Z., Alem, N., Gannett, W. and Zettl, A. (2010). Determination of the Local Chemical Structure of Graphene Oxide and Reduced Graphene Oxide. *Adv. Mater.*, 22(40), pp.4467-4472.

Fang, M., Wang, K., Lu, H., Yang, Y. and Nutt, S. (2009). Covalent polymer functionalization of graphene nanosheets and mechanical properties of composites. *Journal of Materials Chemistry*, 19(38), p.7098.

Fang, M., Zhang, Z., Li, J., Zhang, H., Lu, H. and Yang, Y. (2010). Constructing hierarchically structured interphases for strong and tough epoxy nanocomposites by amine-rich graphene surfaces. *Journal of Materials Chemistry*, 20(43), p.9635.

Fornes, T. and Paul, D. (2003). Formation and properties of nylon 6 nanocomposites. *PolÃ meros*, 13(4).

Fu, X. and Qutubuddin, S. (2001). Polymer–clay nanocomposites: exfoliation of organophilic montmorillonite nanolayers in polystyrene. *Polymer*, 42(2), pp.807-813.

Gao, W., Alemany, L., Ci, L. and Ajayan, P. (2009). New insights into the structure and reduction of graphite oxide. *Nature Chem*, 1(5), pp.403-408.

Geim, A. and Novoselov, K. (2007). The rise of graphene. *Nat Mater*, 6(3), pp.183-191.

Ghosh, A. (2009). *Processing-Structure-Properties Relationship In Polymeric Nanostructured Materials*. [online] Eng.nus.edu.sg. Available at: http://www.eng.nus.edu.sg/nusnni/activities_files/Slides-Anup.Ghosh [Accessed 14 May 2015].

Gonçalves, G., Marques, P., Barros-Timmons, A., Bdkin, I., Singh, M., Emami, N. and Grácio, J. (2010). Graphene oxide modified with PMMA via ATRP as a reinforcement filler. *Journal of Materials Chemistry*, 20(44), p.9927.

Greco, A., Timo, A. and Maffezzoli, A. (2012). Development and Characterization of Amorphous Thermoplastic Matrix Graphene Nanocomposites. *Materials*, 5(12), pp.1972-1985.

Hassani, A., Ishak, Z. and Mohamed, A. (2013). Preparation and characterization of polyamide 6 nanocomposites using MWCNTs based on bimetallic Co-Mo/MgO catalyst. *expresspolymlett*, 8(3), pp.177-186.

Haubner, K., Murawski, J., Olk, P., Eng, L., Ziegler, C., Adolphi, B. and Jaehne, E. (2010). The Route to Functional Graphene Oxide. *ChemPhysChem*, 11(10), pp.2131-2139.

Higginbotham, A., Lomeda, J., Morgan, A. and Tour, J. (2009). Graphite Oxide Flame-Retardant Polymer Nanocomposites. *ACS Appl. Mater. Interfaces*, 1(10), pp.2256-2261.

Horacio J. Salavagione, Gary Ellis, and Gerardo Martinez, (2011). *Graphene-Based Polymer Nanocomposites*. INTECH Open Access Publisher.

Hu, N., Wei, L., Wang, Y., Gao, R., Chai, J., Yang, Z., Kong, E. and Zhang, Y. (2011). Graphene Oxide Reinforced Polyimide Nanocomposites via In Situ Polymerization. *Journal of Nanoscience and Nanotechnology*, 11, pp.1-6.

Hummers, W. and Offeman, R. (1958). Preparation of Graphitic Oxide. *J. Am. Chem. Soc.*, 80(6), pp.1339-1339.

Jin, J., Rafiq, R., Gill, Y. and Song, M. (2013). Preparation and characterization of high performance of graphene/nylon nanocomposites. *European Polymer Journal*, 49(9), pp.2617-2626.

Kilbride, B., Coleman, J., Fraysse, J., Fournet, P., Cadek, M., Drury, A., Hutzler, S., Roth, S. and Blau, W. (2002). Experimental observation of scaling laws for alternating current and direct current conductivity in polymer-carbon nanotube composite thin films. *J. Appl. Phys.*, 92(7), p.4024.

Kim, H. and Macosko, C. (2009). Processing-property relationships of polycarbonate/graphene composites. *Polymer*, 50(15), pp.3797-3809.

Kim, J., Cote, L. and Huang, J. (2012). Two Dimensional Soft Material: New Faces of Graphene Oxide.*Acc. Chem. Res.*, 45(8), pp.1356-1364.

Lee, C., Wei, X., Kysar, J. and Hone, J. (2008). Measurement of the Elastic Properties and Intrinsic Strength of Monolayer Graphene. *Science*, 321(5887), pp.385-388.

Lerf, A., He, H., Forster, M. and Klinowski, J. (1998). Structure of Graphite Oxide Revisited ‖. *J. Phys. Chem. B*, 102(23), pp.4477-4482.

Li, J., Zeng, X., Ren, T. and van der Heide, E. (2014). The Preparation of Graphene Oxide and Its Derivatives and Their Application in Bio-Tribological Systems. *Lubricants*, 2(3), pp.137-161.

Liang, Y., Logsdon, J., Cho, J. and Lan, T. (2001). NANOEFFECT IN IN SITU NYLON6 NANOCOMPOSITES. [online] Available at: http://www.nanocor.com/tech_papers/antec2001.asp [Accessed 3 Feb. 2015].

Liu, T., Ping Lim, K., Chauhari Tjiu, W., Pramoda, K. and Chen, Z. (2003). Preparation and characterization of nylon 11/organoclay nanocomposites. *Polymer*, 44(12), pp.3529-3535.

Madaleno, L., Schjødt-Thomsen, J. and Pinto, J. (2010). Morphology, thermal and mechanical properties of PVC/MMT nanocomposites prepared by solution blending and solution blending+melt compounding. *Composites Science and Technology*, 70(5), pp.804-814.

Marques, P., Goncalves, G., Cruz, S., Almeida, N., Singh, M., Gracio, J. and Sousa, A. (2011). Functionalized Graphene Nanocomposites. *Advances in Nanocomposite Technology*.

Mert, M. (2007). *IMPACT MODIFIED NYLON 66-ORGANOCLAY NANOCOMPOSITES*. [online] pp.135-136. Available at: https://etd.lib.metu.edu.tr/upload/12608112/index.pdf [Accessed 17 May 2015].

McAllister, M., Li, J., Adamson, D., Schniepp, H., Abdala, A., Liu, J., Herrera-Alonso, M., Milius, D., Car, R., Prud'homme, R. and Aksay, I. (2007). Single Sheet Functionalized Graphene by Oxidation and Thermal Expansion of Graphite. *Chem. Mater.*, 19(18), pp.4396-4404.

Mikhailov, S. (2011). *Physics and applications of graphene*. Rijeka: InTech, pp.169-188.

Morimune, S., Nishino, T. and Goto, T. (2012). Poly(vinyl alcohol)/graphene oxide nanocomposites prepared by a simple eco-process. *Polym J*, 44(10), pp.1056-1063.

Naffakh, M., Marco, C., Gómez, M. and Jiménez, I. (2011). Novel melt-processable nylon-6/inorganic fullerene-like WS2 nanocomposites for critical applications. *Materials Chemistry and Physics*, 129(1-2), pp.641-648.

Nakajima, T. and Matsuo, Y. (1994). Formation process and structure of graphite oxide. *Carbon*, 32(3), pp.469-475.

Nakajima, T., Mabuchi, A. and Hagiwara, R. (1988). A new structure model of graphite oxide. *Carbon*, 26(3), pp.357-361.

Nanocvd.co.uk, (2015). *Graphene - nanoCVD.co.uk*. [online] Available at: http://www.nanocvd.co.uk/graphene_introduction_nanoCVD.html [Accessed 12 Feb. 2015].

Nguyen, D., Lee, Y., Raghu, A., Jeong, H., Shin, C. and Kim, B. (2009). Morphological and physical properties of a thermoplastic polyurethane reinforced with functionalized graphene sheet. *Polym. Int.*, 58(4), pp.412-417.

Niyogi, S., Bekyarova, E., Itkis, M., McWilliams, J., Hamon, M. and Haddon, R. (2006). Solution Properties of Graphite and Graphene. *J. Am. Chem. Soc.*, 128(24), pp.7720-7721.

O'Neill, A., Bakirtzis, D. and Dixon, D. (2014). Polyamide 6/Graphene composites: The effect of in situ polymerisation on the structure and properties of graphene oxide and reduced graphene oxide.*European Polymer Journal*, 59, pp.353-362.

Pandey, J., Reddy, K., Mohanty, A. and Misra, M. (2014). *Handbook of Polymernanocomposites. Processing, Performance and Application*. Dordrecht: Springer, p.530.

Papageorgiou, G., Terzopoulou, Z., Achilias, D., Triantafyllidis,, K., Bikiaris, D., Diamanti, E. and Gournis, D. (2013). Poly(Ethylene Succinate)/Graphene Oxide Nanocomposites - Preparation And Characterization. [online] Available at: http://9pesxm.chemeng.ntua.gr/fullpapers/MP0342.pdf [Accessed 22 Feb. 2015]

Paredes, J., Villar-Rodil, S., Martínez-Alonso, A. and Tascón, J. (2008). Graphene Oxide Dispersions in Organic Solvents. *Langmuir*, 24(19), pp.10560-10564.

Park, S. and Ruoff, R. (2009). Chemical methods for the production of graphenes. *Nature Nanotech*, 4(4), pp.217-224.

Paul, D. and Robeson, L. (2008). Polymer nanotechnology: Nanocomposites. *Polymer*, 49(15), pp.3187-3204.

Phlegm, H. (2009). *The role of the chemist in automotive design*. Boca Raton, FL: CRC Press/Taylor & Francis, p.42.

Pokharel, P., Choi, S. and Lee, D. (2015). The effect of hard segment length on the thermal and mechanical properties of polyurethane/graphene oxide nanocomposites. *Composites Part A: Applied Science and Manufacturing*, 69, pp.168-177.

Potts, J., Dreyer, D., Bielawski, C. and Ruoff, R. (2011). Graphene-based polymer nanocomposites.*Polymer*, 52(1), pp.5-25.

Rafiee, M., Rafiee, J., Srivastava, I., Wang, Z., Song, H., Yu, Z. and Koratkar, N. (2010). Fracture and Fatigue in Graphene Nanocomposites. *Small*, 6(2), pp.179-183.

Raidongia, K., Tan, A. and Huang, J. (2014). Graphene Oxide: Some New Insights into an Old Material. *Carbon Nanotubes and Graphene*, pp.341-374.

Ramanathan, T., Abdala, A., Stankovich, S., Dikin, D., Herrera-Alonso, M., Piner, R., Adamson, D., Schniepp, H., Chen, X., Ruoff, R., Nguyen, S., Aksay, I., Prud'Homme, R. and Brinson, L. (2008). Functionalized graphene sheets for polymer nanocomposites. *Nature Nanotech*, 3(6), pp.327-331.

Ramanathan, T., Abdala, A., Stankovich, S., Dikin, D., Herrera-Alonso, M., Piner, R., Adamson, D., Schniepp, H., Chen, X., Ruoff, R., Nguyen, S., Aksay, I.,

Prud'Homme, R. and Brinson, L. (2008). Functionalized graphene sheets for polymer nanocomposites. *Nature Nanotech*, 3(6), pp.327-331.

Rangari, V., Shaik, M., Mahfuz, H. and Jeelani, S. (2009). Fabrication and characterization of high strength Nylon-6/Si3N4 polymer nanocomposite fibers. *Materials Science and Engineering: A*, 500(1-2), pp.92-97.

Raza, H. (2012). *Graphene nanoelectronics*. Berlin: Springer, p.437.

Rigaku.com, (2015). *Percent crystallinity of polymers | Rigaku - X-ray analytical instrumentation*. [online] Available at: http://www.rigaku.com/en/products/xrd/rapid/app003 [Accessed 24 May 2015].

Rlhudson.com, (2015). *THERMOSET VS THERMOPLASTIC*. [online] Available at: http://www.rlhudson.com/thermoplastic-vs-thermoset.html [Accessed 11 Feb. 2015].

Rtpcompany.com, (2015). *Nylon 6 (PA) — Polyamide 6*. [online] Available at: http://www.rtpcompany.com/products/product-guide/nylon-6-pa-polyamide-6/ [Accessed 1 Feb. 2015].

Salehi, S., Ehsani, M. and Khonakdar, H. (2015). Assessment of thermal, morphological, and mechanical properties of poly(methyl methacrylate)/glass flake composites. *Journal of Vinyl and Additive Technology*, p.n/a-n/a.

Sangwan, P., Way, C. and Wu, D. (2009). New insight into biodegradation of polylactide (PLA)/clay nanocomposites using molecular ecological techniques. *Macromol. Biosci.*, 9(7), pp.677–686.

Scharfenberg, S., Rocklin, D., Chialvo, C., Weaver, R., Goldbart, P. and Mason, N. (2011). Probing the mechanical properties of graphene using a corrugated elastic substrate. *Applied Physics Letters*, 98(9), p.091908.

Sengupta, R., Bhattacharya, M., Bandyopadhyayb, S. and Bhowmick, A. (2011). A review on the mechanical and electrical properties of graphite and modified graphite reinforced polymer composites. *Prog. Polym. Sci.*, 36(5), pp.638-670.

Si, Y. and Samulski, E. (2008). Synthesis of Water Soluble Graphene. *Nano Letters*, 8(6), pp.1679-1682.

Song, J., Wang, X. and Chang, C. (2014). Preparation and Characterization of Graphene Oxide. *Journal of Nanomaterials*, 2014, pp.1-6.

Srivastava, I., Mehta, R., Yu, Z., Schadler, L. and Koratkar, N. (2011). Raman study of interfacial load transfer in graphene nanocomposites. *Applied Physics Letters*, 98(6), p.063102.

Stankovich, S., Dikin, D., Dommett, G., Kohlhaas, K., Zimney, E., Stach, E., Piner, R., Nguyen, S. and Ruoff, R. (2006). Graphene-based composite materials. *Nature*, 442(7100), pp.282-286.

Su, C. and Loh, K. (2013). Carbocatalysts: Graphene Oxide and Its Derivatives. *Acc. Chem. Res.*, 46(10), pp.2275-2285.

Suñer, S., Joffe, R., Tipper, J. and Emami, N. (2015). Ultra high molecular weight polyethylene/graphene oxide nanocomposites: Thermal, mechanical and wettability characterisation.*Composites Part B: Engineering*, 78, pp.185-191.

Tanasa, F. and Zanoaga, M. (2014). Study of Properties of Some Polyethylene-Clay Nanocomposites: Influence of Preparation Method on the Degree of Clay Intercalation/Exfoliation. *Chemistry Journal of Moldova. General, Industrial and Ecological Chemistry*, 9(1), pp.106-111.

Tayebi, M., Ramazani S.A, A., Hamed Mosavian, M. and Tayyebi, A. (2015). LDPE/EVA/graphene nanocomposites with enhanced mechanical and gas permeability properties. *Polym. Adv. Technol.*, p.n/a-n/a.

Thostenson, E., Li, C. and Chou, T. (2005). Nanocomposites in context. *Composites Science and Technology*, 65(3-4), pp.491-516.

Tripathi, S., Saini, P., Gupta, D. and Choudhary, V. (2013). Electrical and mechanical properties of PMMA/reduced graphene oxide nanocomposites prepared via in situ polymerization. *J Mater Sci*, 48(18), pp.6223-6232.

Usuki, A., Kojima, Y., Kawasumi, M., Okada, A., Fukushima, Y., Kurauchi, T. and Kamigaito, O. (1993). Synthesis of nylon 6-clay hybrid. *Journal of Materials Research*, 8(05), pp.1179-1184.

Wakabayashi, K., Pierre, C., Dikin, D., Ruoff, R., Ramanathan, T., Brinson, L. and Torkelson, J. (2008). Polymer−Graphite Nanocomposites: Effective Dispersion and Major Property Enhancement via Solid-State Shear Pulverization. *Macromolecules*, 41(6), pp.1905-1908.

Wang, C., Wu, H. and Qian, Y. (2015). Preparation and Mechanical Properties of Graphene Reinforced Poly(vinyl alcohol) Nanocomposites. *Asian Journal of Chemistry*, 27(2), pp.744-748.

Wang, M., Yan, C. and Ma, L. (2012). Graphene Nanocomposites. *Composites and Their Properties*. [online] Available at: http://www.intechopen.com/books/composites-and-their-properties/graphene-nanocomposites [Accessed 29 Jan. 2015].

Wu, T. and Ting, J. (2013). Preparation and characteristics of graphene oxide and its thin films. *Surface and Coatings Technology*, 231, pp.487-491.

Xu, Y., Hong, W., Bai, H., Li, C. and Shi, G. (2009). Strong and ductile poly(vinyl alcohol)/graphene oxide composite films with a layered structure. *Carbon*, 47(15), pp.3538-3543.

Xu, Z. and Gao, C. (2010). In situ Polymerization Approach to Graphene-Reinforced Nylon-6 Composites. *Macromolecules*, 43(16), pp.6716-6723.

Yang, H., Shan, C., Li, F., Zhang, Q., Han, D. and Niu, L. (2009). Convenient preparation of tunably loaded chemically converted graphene oxide/epoxy resin nanocomposites from graphene oxide sheets through two-phase extraction. *Journal of Materials Chemistry*, 19(46), p.8856.

Zhang, N., Wang, L., Liu, H. and Cai, Q. (2008). Nitric acid oxidation on carbon dispersion and suspension stability. *Surf. Interface Anal.*, 40(8), pp.1190-1194.

Zhang, X., Fan, X., Li, H. and Yan, C. (2012). Facile preparation route for graphene oxide reinforced polyamide 6 composites via in situ anionic ring-opening polymerization. *Journal of Materials Chemistry*, 22(45), p.24081.

Zhao, X., Zhang, Q., Chen, D. and Lu, P. (2010). Enhanced Mechanical Properties of Graphene-Based Poly(vinyl alcohol) Composites. *Macromolecules*, 43(5), pp.2357-2363.

Zhu, J., Kim, J., Peng, H., Margrave, J., Khabashesku, V. and Barrera, E. (2003). Improving the Dispersion and Integration of Single-Walled Carbon Nanotubes in Epoxy Composites through Functionalization. *Nano Letters*, 3(8), pp.1107-1113.

Zhu, Y., Murali, S., Cai, W., Li, X., Suk, J., Potts, J. and Ruoff, R. (2010). Graphene and Graphene Oxide: Synthesis, Properties, and Applications. *Adv. Mater.*, 22(35), pp.3906-3924.

Zhu, Y., Murali, S., Stoller, M., Velamakanni, A., Piner, R. and Ruoff, R. (2010). Microwave assisted exfoliation and reduction of graphite oxide for ultracapacitors. *Carbon*, 48(7), pp.2118-2122.

APPENDICES

APPENDIX A: X-Ray Diffraction

(a) XRD Diffractogram of GNF and Graphite Oxide

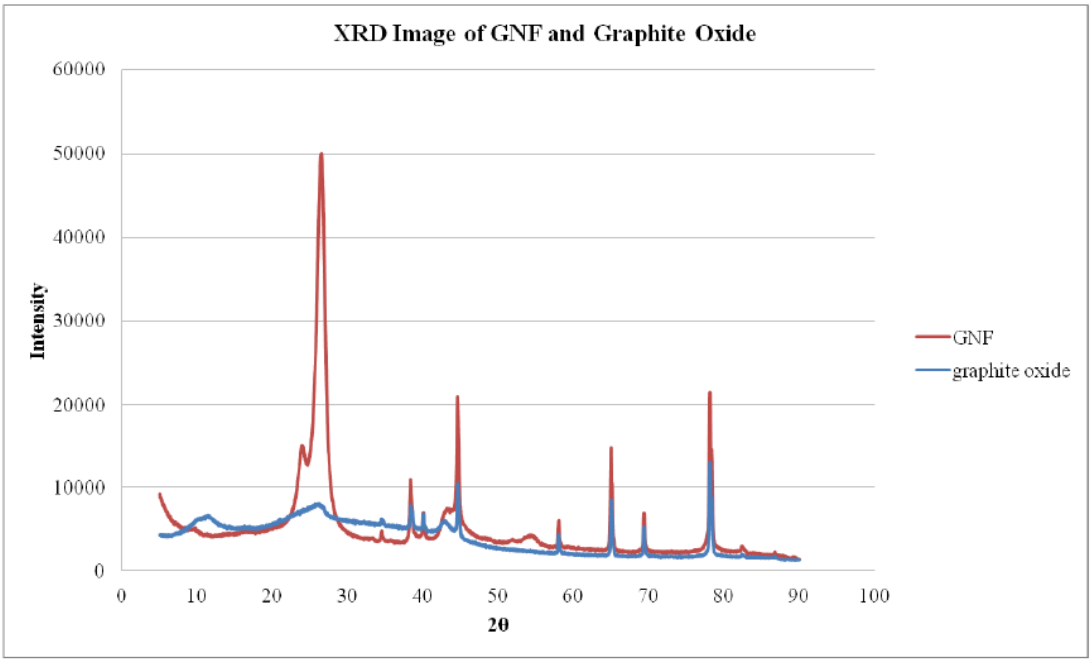

APPENDIX B: Fourier Transform Infrared Spectroscopy

(a) Nylon-6

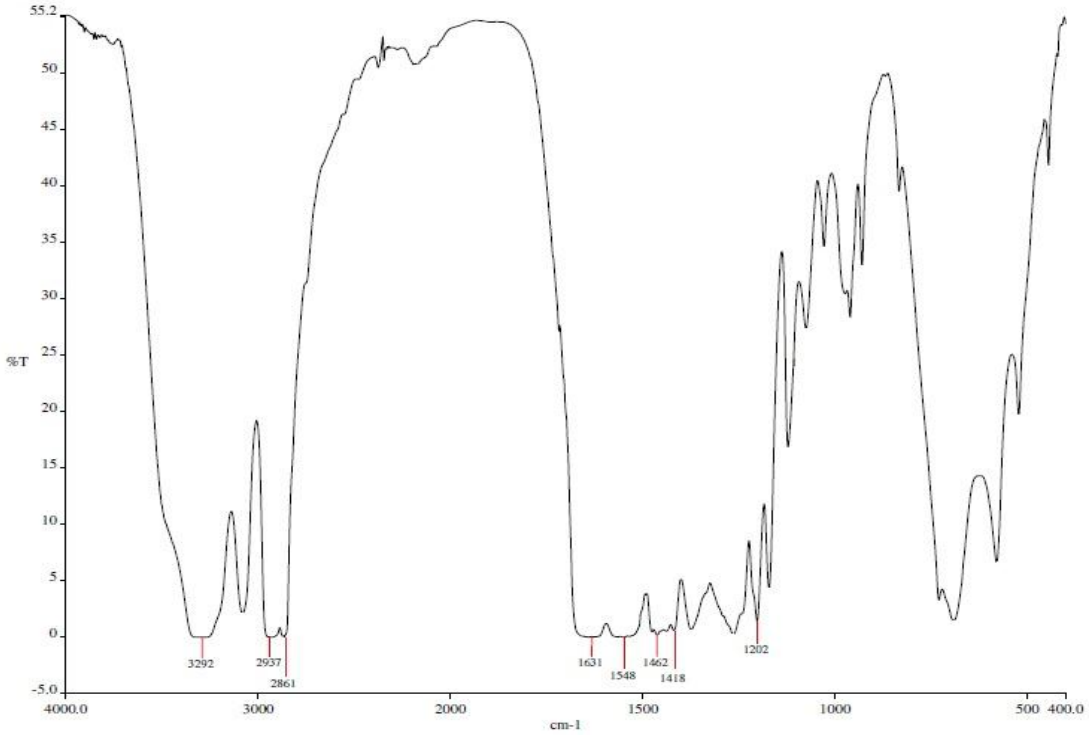

(b) Nylon-6/0.5wt%GO

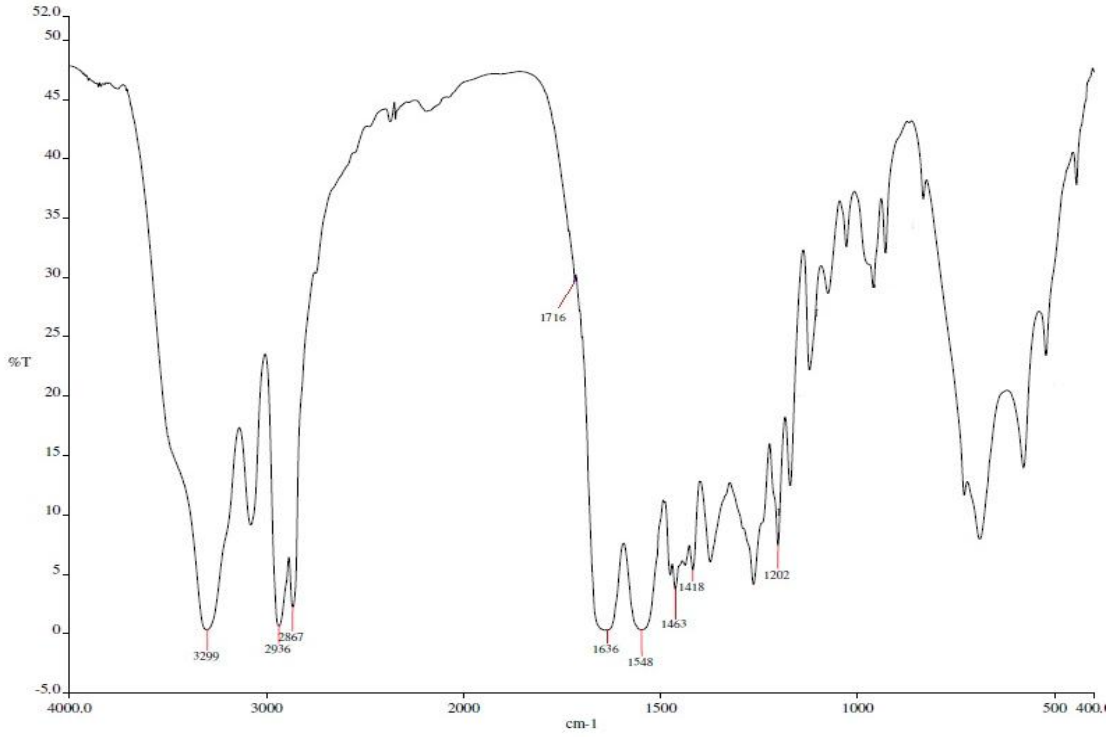

(c) Nylon-6/1.0wt%GO

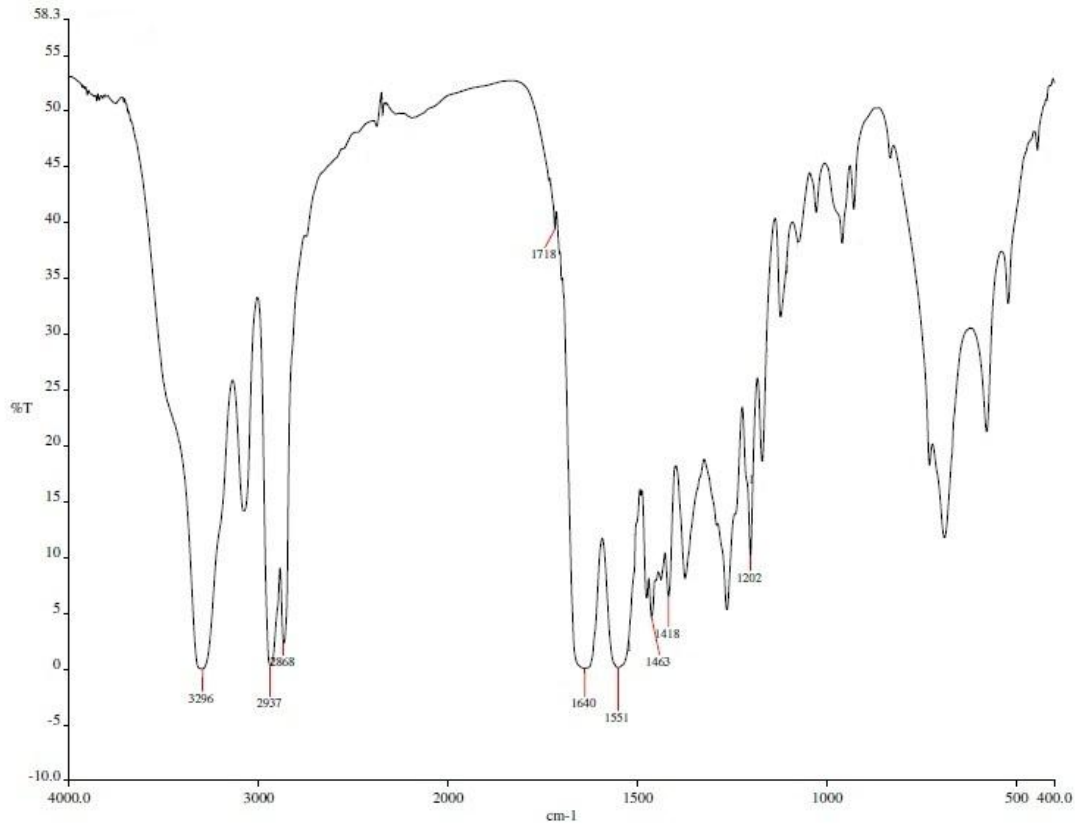

(d) Nylon-6/1.5wt%GO

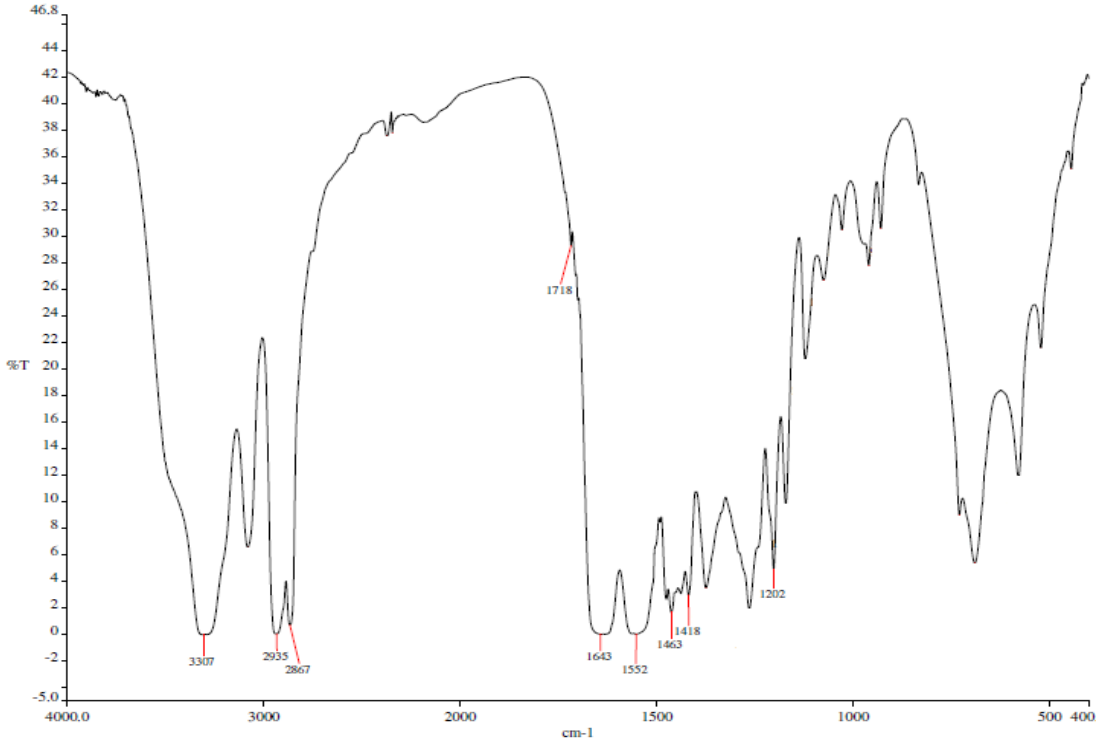

(e) Nylon-6/2.0wt%GO

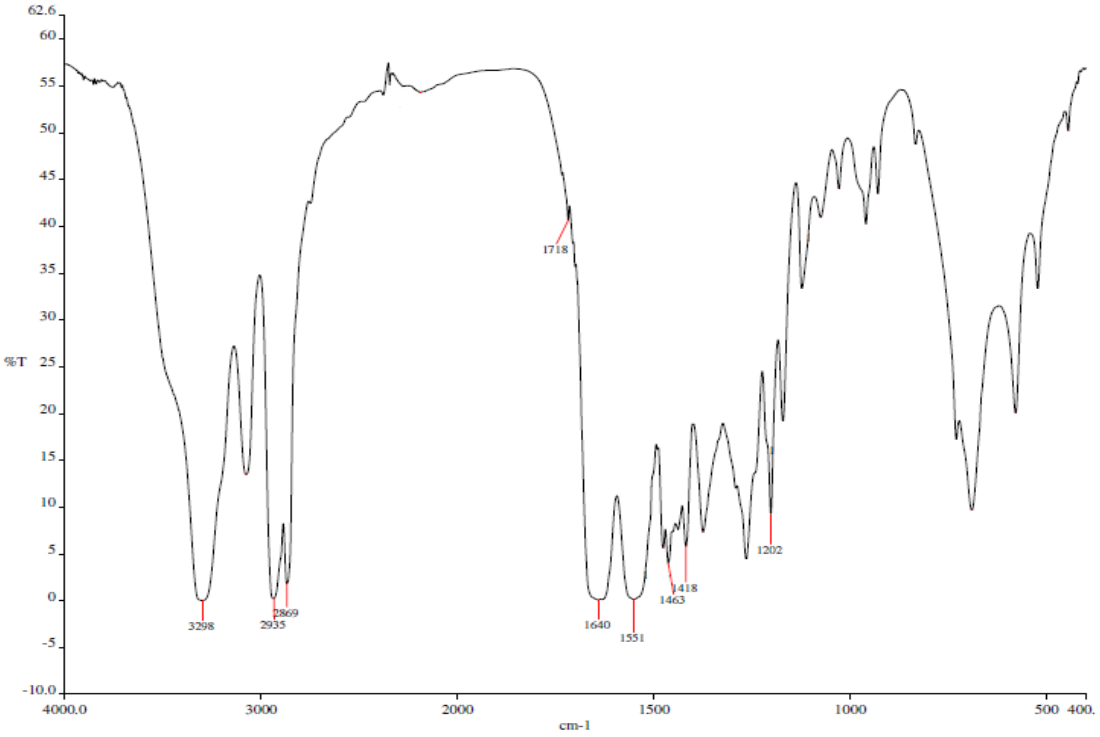

APPENDIX C: Differential Scanning Calorimetry

(a) Nylon-6

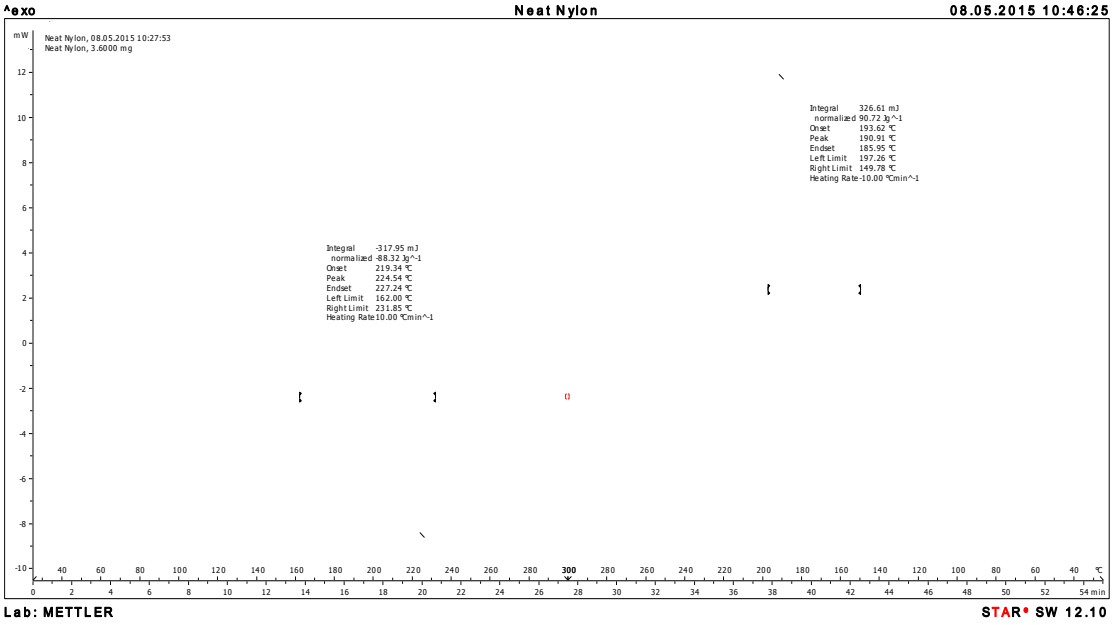

(b) Nylon-6/0.5wt%

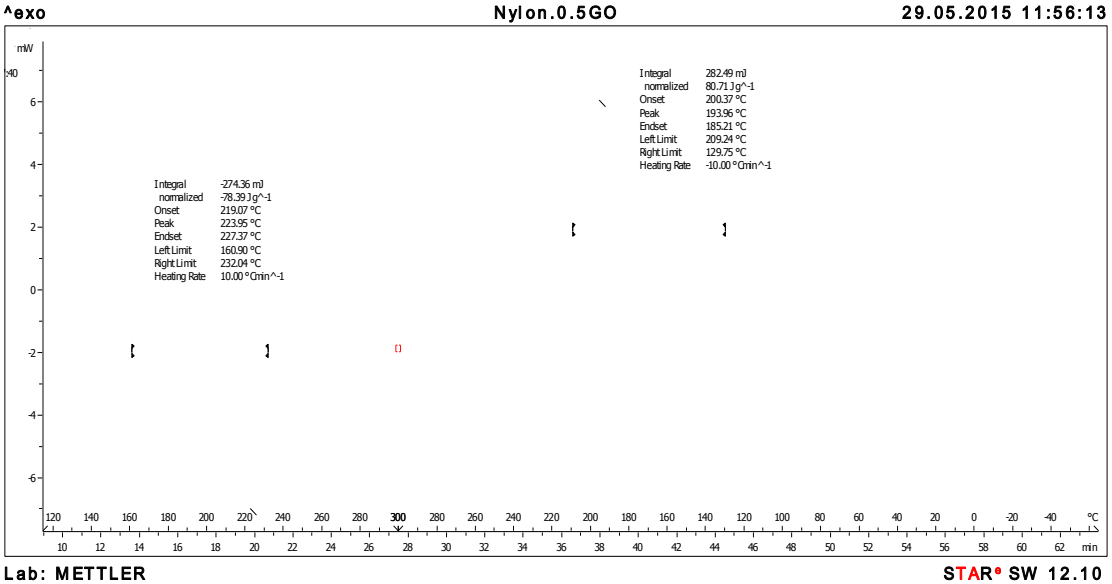

(c) Nylon-6/1.0wt%GO

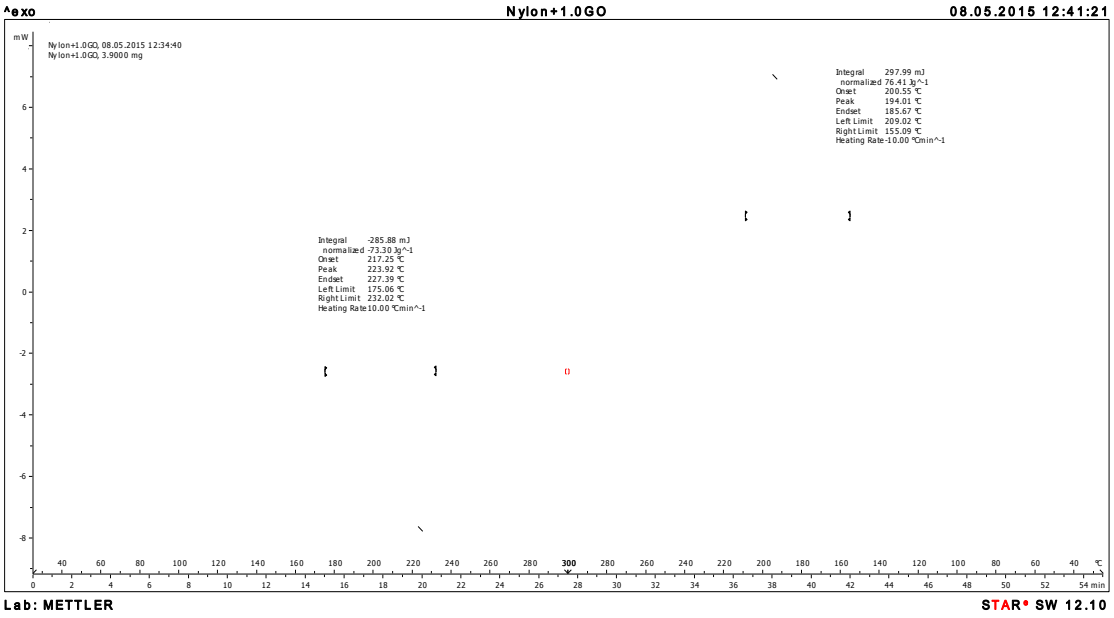

(d) Nylon-6/1.5wt%GO

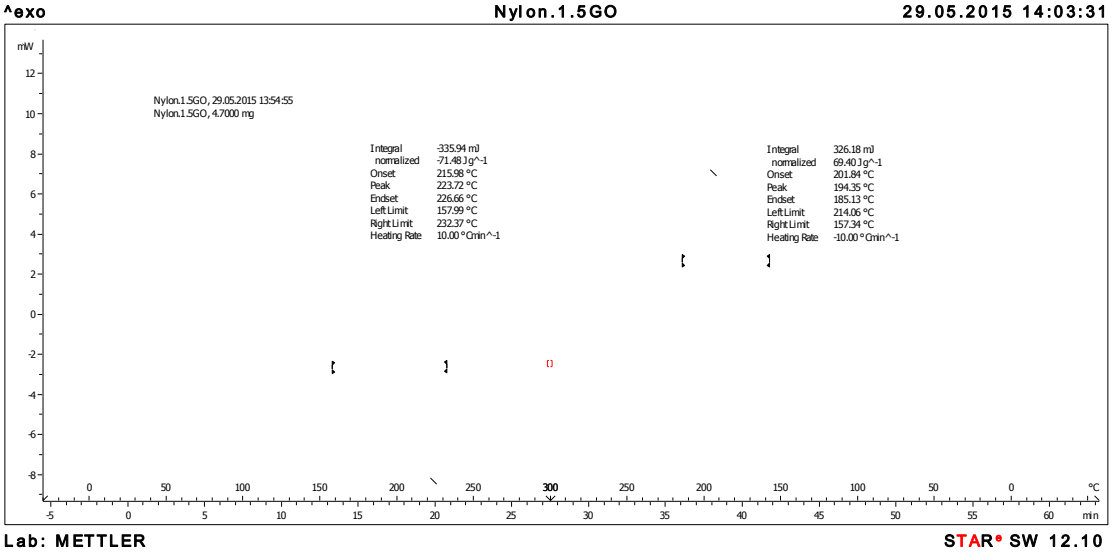

(e) Nylon-6/2.0wt%GO

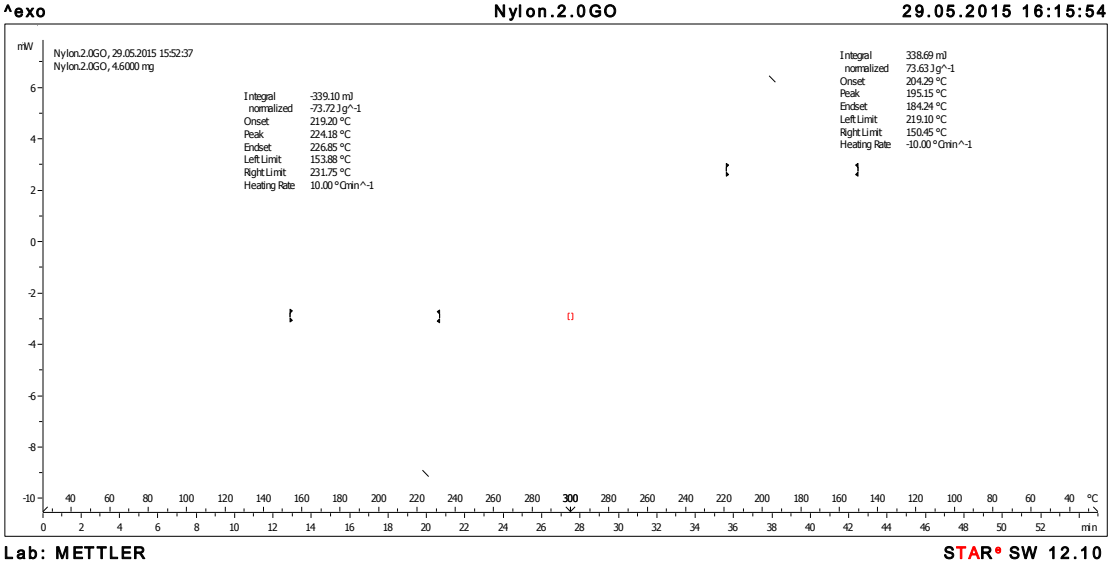

APPENDIX D: Thermal Gravimetric Analysis

(a) Nylon-6

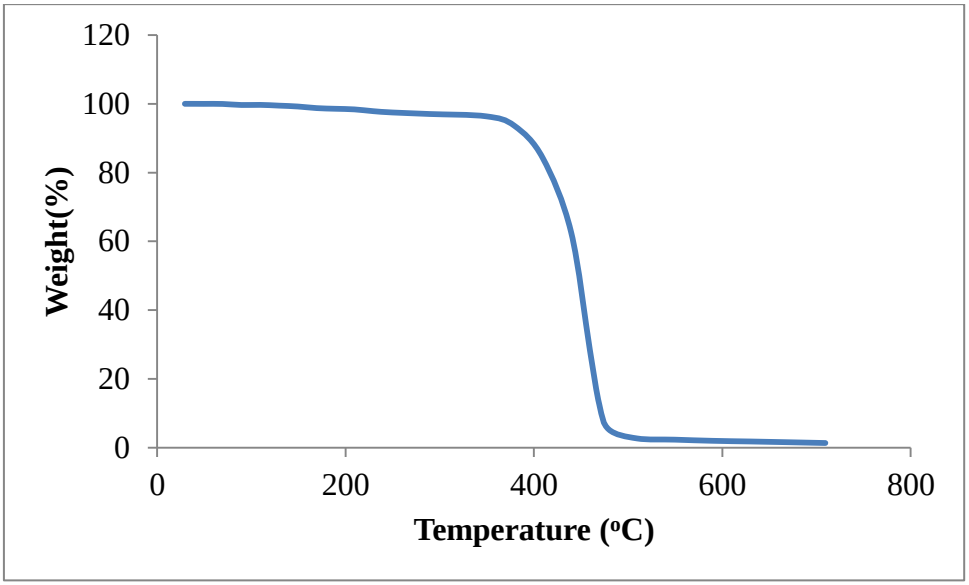

(b) Nylon-6/0.5wt%GO

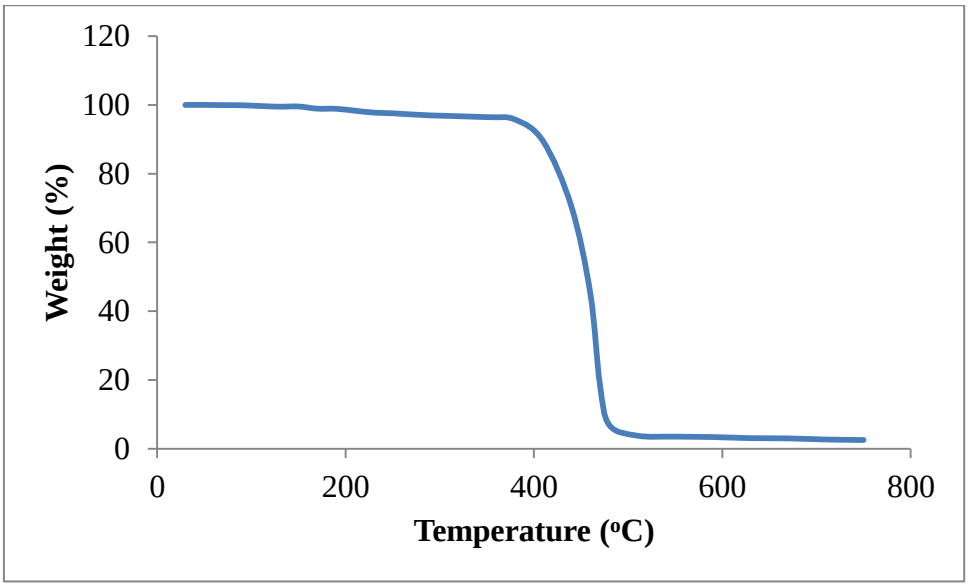

(c) Nylon-6/1.0wt%GO

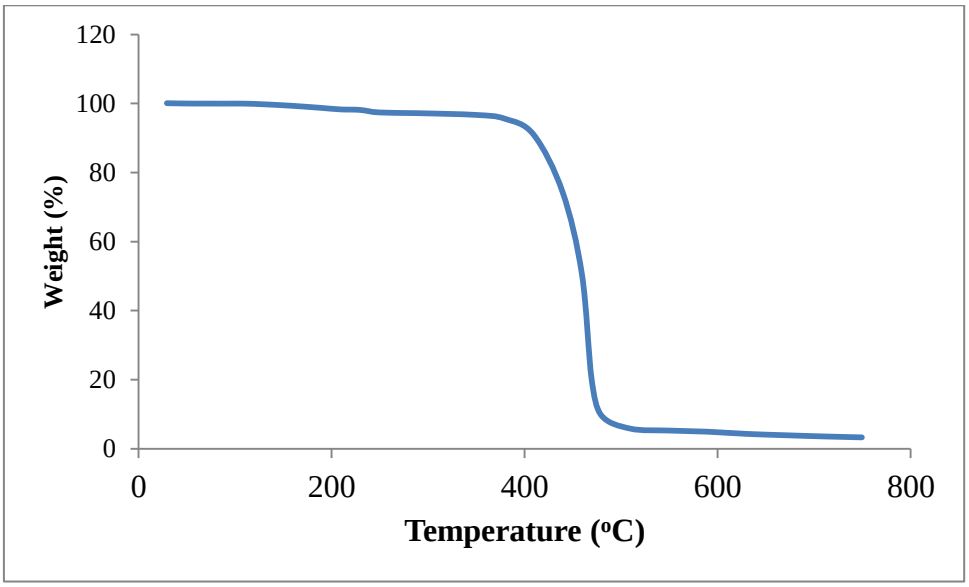

(d) Nylon-6/1.5wt%GO

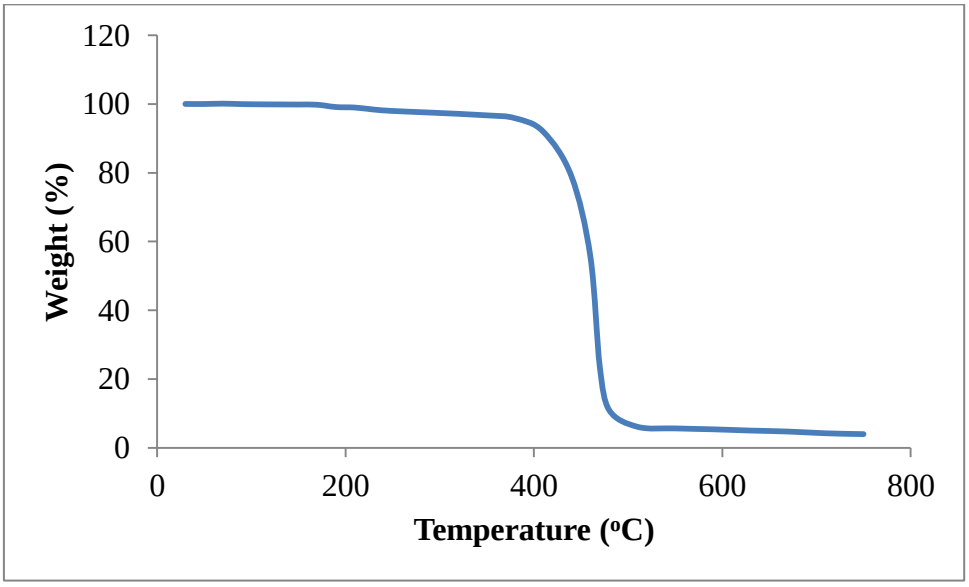

(e) Nylon-6/2.0wt%GO

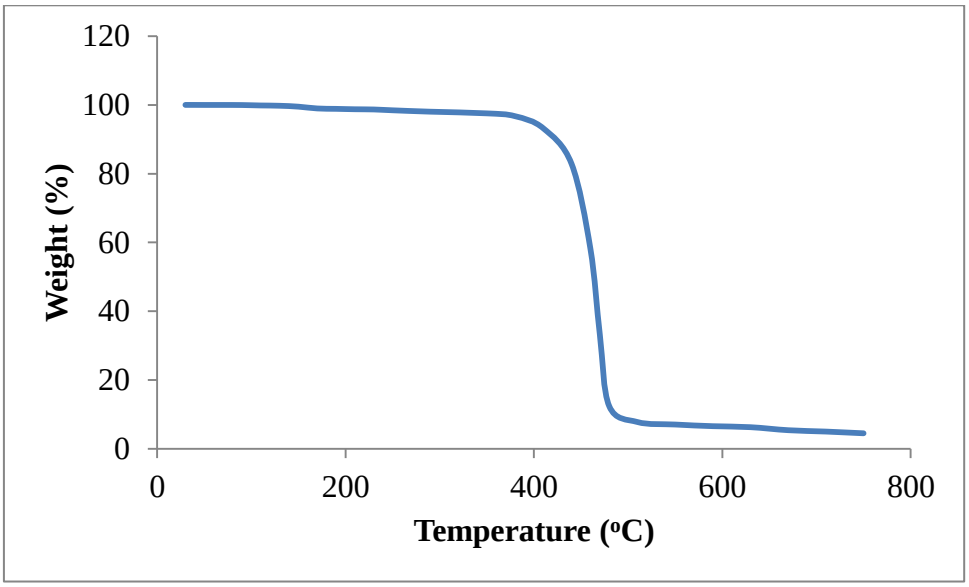

APPENDIX E: Receipt of Manuscript Submission to Journal of Polymer Testing

Elsevier Editorial System(tm) for Polymer Testing

Manuscript Draft

Manuscript Number: POTE-D-15-00715

Title: DEVELOPMENT OF GRAPHENE OXIDE/NYLON-6 HIGH PERFORMANCE NANOCOMPOSITES

Article Type: Original Paper

Keywords: Graphene; Graphene oxide; Nylon-6; Nanocomposite; Thermal Properties

Corresponding Author: Dr. Yamuna Munusamy, PhD

Corresponding Author's Institution: Universiti Tunku Abdul Rahman

First Author: Yamuna Munusamy, PhD

Order of Authors: Yamuna Munusamy, PhD; Yi Hui Tay, Bachelor ; Mathialagan Muniyadi, PhD

Suggested Reviewers: Beng Teik Poh PhD
Associate Professor, School of Industrial Technology, Universiti Sains Malaysia
btpoh@usm.my

Che Husna Azahari PhD
Professor, Mechanical and Material Engineering Department, Universiti Kebangsaan Malaysia (UKM),
Mek@ulsi.eng.ukm.my

Chakrit Sirisinha PhD
Associate Professor, Faculty of Science, Mahidol University, Salaya Campus
sccsr@mahidol.ac.th

Opposed Reviewers: